

Phenotypic and Genetic Characteristics of Retinal Vascular Parameters and their Association with Diseases

Sofía Ortín Vela*[†]^{1,2}, Michael J. Beyeler*[†]^{1,2}, Olga Trofimova^{1,2}, Ilaria Iuliani^{1,2}, Jose D. Vargas Quiros^{3,4}, Victor A. de Vries^{3,4}, Ilenia Meloni⁵, Adham Elwakil⁵, Florence Hoogewoud⁵, Bart Liefers^{3,4}, David Presby^{1,2}, Wishal D. Ramdas³, Mattia Tomasoni⁵, Reinier Schlingemann^{5,6}, Caroline C.W. Klaver^{3,4,7,8}, and Sven Bergmann[†]^{1,2,9}

¹Dept. of Computational Biology, University of Lausanne, Lausanne, Switzerland

²Swiss Institute of Bioinformatics, Lausanne, Switzerland

³Department of Ophthalmology, Erasmus MC University Medical Center, Rotterdam, The Netherlands

⁴Department of Epidemiology, Erasmus MC University Medical Center, Rotterdam, The Netherlands

⁵Jules-Gonin Eye Hospital, FAA, University of Lausanne, Lausanne, Switzerland

⁶Department of Ophthalmology, Amsterdam University Medical Centres, Amsterdam, The Netherlands

⁷Department of Ophthalmology, Radboud University Medical Center, Nijmegen, The Netherlands

⁸Institute of Molecular and Clinical Ophthalmology, University of Basel, Basel, Switzerland

⁹Dept. of Integrative Biomedical Sciences, University of Cape Town, Cape Town, South Africa

Abstract

Fundus images allow for non-invasive assessment of the retinal vasculature whose features provide important information on health. Using a fully automated image processing pipeline, we extracted 17 different morphological vascular phenotypes, including median vessels diameter, diameter variability, main temporal angles, vascular density, central retinal equivalents, the number of bifurcations, and tortuosity, from over 130k fundus images of close to 72k UK Biobank subjects. We performed Genome-Wide Association Studies of these phenotypes. From this, we estimated their heritabilities, ranging between 5 and 25%, and genetic cross-phenotype correlations, which mostly mirrored the corresponding phenotypic correlations, but tended to be slightly larger. Projecting our genetic association signals onto genes and pathways revealed remarkably low overlap suggesting largely decoupled mechanisms modulating the different phenotypes. Our disease phenotype associations confirmed some previously known findings and revealed many novel connections. Notably, diameter variability, especially for the veins, seems to have new and interesting associations with diseases, including heart attack, pulmonary embolism, and age of death. Mendelian Randomization analysis suggests a causal influence of blood pressure and body mass index on retinal vessel morphology, among other results. We validated key findings in two independent smaller

*Equal first authors in random order

[†]E-mails: sofia.ortinvela@unil.ch, michael.beyeler@unil.ch, sven.bergmann@unil.ch

NOTE: This preprint reports new research that has not been certified by peer review and should not be used to guide clinical practice.

32 cohorts. Our analyses provide evidence that large-scale analysis of image-derived vascular phenotypes
33 has sufficient power for obtaining functional, as well as some initial causal insights into the processes
34 modulating the retinal vasculature.

35 **Keywords:** GWAS, retina, CFI, IDPs, vasculature, genes, vascular diseases, heritability, MR.

36 **Nonstandard Abbreviations and Acronyms**

- 37 BMI: Body mass index
- 38 CFI: Color fundus image
- 39 CNN: Convolutional neural network
- 40 DBP: Diastolic blood pressure
- 41 DL: Deep learning
- 42 DVT: Deep vein thrombosis
- 43 ED: Eye diseases
- 44 FDR: False discovery rate
- 45 HDL: High-density lipoprotein
- 46 HbA1c: Glycated hemoglobin
- 47 IDP: Image-derived phenotype
- 48 IVW: Inverse variance weighted
- 49 LDL: Low-density lipoprotein
- 50 LDSR: Linkage disequilibrium score regression
- 51 LOO: Leave-one-out
- 52 LWNET: Little W-Net
- 53 MR: Mendelian Randomisation
- 54 OD: Optic disc
- 55 PAD: Peripheral artery disease
- 56 PC: Principal component
- 57 PE: Pulmonary embolism
- 58 PR: Pulse rate
- 59 PWASI: Pulse wave arterial stiffness index
- 60 QC: Quality control
- 61 RS: Rotterdam Study
- 62 SBP: Systolic blood pressure
- 63 SNP: Single nucleotide polymorphism
- 64 UKBB: UK Biobank

65 Introduction

66 The retina provides a unique opportunity for imaging human vasculature. In particular, retinal color fundus
67 images (CFIs) allow for noninvasive in-vivo assessment of the vascular system of the superficial inner layer
68 of the retina. Such images have been acquired in several cohorts and there is a large body of research on
69 automatic extraction of vascular properties and their associations with medically relevant information.

70 It is well established that vascular properties obtained from retinal imaging not only enable the monitoring
71 of ocular diseases such as diabetic retinopathy, macular degeneration, and glaucoma, but can also serve
72 as a powerful screening tool for early detection of systemic diseases, including stroke [1–4], coronary heart
73 disease [5, 6], peripheral artery diseases [7], hypertension [3, 4, 8–18], atherosclerosis [2, 3, 19], and myocardial
74 infarction [20, 21]. Retinal abnormalities have also been associated with common comorbidities such as
75 diabetes [8, 22–24] and obesity [25].

76 The processing of CFIs typically can be divided into three steps. First, the image is processed at the level
77 of pixels to identify which of them represents blood vessels (possibly distinguishing between arteries and
78 veins), or other structures, like the optic disc (OD). In the second step this pixel-wise information is used
79 to annotate the retina in terms of objects, such as vessel segments represented as a list of points along their
80 midline, as well as the vessel widths along these points. Finally, the information from these objects is used to
81 measure different vascular properties such as vessel diameter or tortuosity, number of bifurcations, as well as
82 certain angles between major vessels. Some simple vascular phenotypes, such as vascular density or fractal
83 dimension, can also be computed directly from the pixel-wise information.

84 While there have been several studies analysing retinal vascular phenotypes [26–31], most of them focused
85 on measuring just one or few retinal phenotypes, often in small image sets, and some required expert input
86 rather than being fully automated [32–34]. Furthermore, the software used for vascular phenotyping is
87 usually not openly accessible, with one very recent exception [35]. Together this precludes the establishment
88 of a comprehensive and reproducible characterisation of large retinal image collections.

89 Recently, Deep Learning (DL) approaches have gained popularity in retinal image analysis. The first con-
90 tribution is at the level of pixel-wise annotation, where state-of-the-art segmentation can be achieved with
91 Convolutional Neural Network (CNN) architectures. For example, the little W-Net (LWNET) annotates pix-
92 els as being part of an artery or vein, outperforming classical segmentation approaches [36]. Such networks
93 can also be used to annotate pixels belonging to the OD [37], vessel bifurcations [38], or other structures.
94 The second contribution of deep CNNs is to learn latent variables providing efficient low-dimensional rep-
95 resentations of retinal images [39, 40]. Such self-supervised, image-based phenotyping can generate novel
96 phenotypes complementing explicit retinal features. Finally, DL approaches have been used to directly
97 predict health-relevant phenotypes from retinal images [41, 42].

98 Beyond their value for assessing ocular or systemic health, retinal phenotypes have also been used in
99 Genome-Wide Association Studies (GWAS) to identify genetic variants modulating these phenotypes. How-

100 ever, previous GWAS have focused on a limited set of vascular properties, such as vessel diameter [43–
101 46], tortuosity [47, 48], vascular density, fractal dimension [49], and certain deep latent variables [39] (see
102 Suppl. Text “Comparison with previous GWAS”).

103 In this study, we present the first joint analysis of 17 retinal vascular phenotypes, including novel features like
104 temporal angles, number of bifurcations, or diameter variability, which have not been analyzed previously at a
105 large scale. Leveraging data from the UK Biobank (UKBB), and employing our open-source fully automated
106 analysis platform, we provide retinal vascular phenotyping for close to 72k subjects, after quality control
107 (QC). For all phenotypes, we performed GWAS, heritability estimates, gene and pathway analyses, as well
108 as associations with a broad set of systemic and ocular diseases. This allowed us to compare cross-phenotype
109 correlations, both at the phenotypic and genotypic levels, study in detail which genes affect individual or
110 multiple phenotypes, and identify potential causal relationships with diseases (see Fig. 1 depicting the overall
111 methodology of our discovery study). We reproduced the phenotypic correlation structure in two independent
112 smaller cohorts: the Rotterdam Study (RS, N=8.1k) and OphtalmoLaus (N=2.2k) participants. Analysis of
113 RS data also provided consistent estimates for phenotypes heritabilities and genetic correlations, as well as
114 replication of a large number of our genome-wide significant hits for the vast majority of phenotypes.

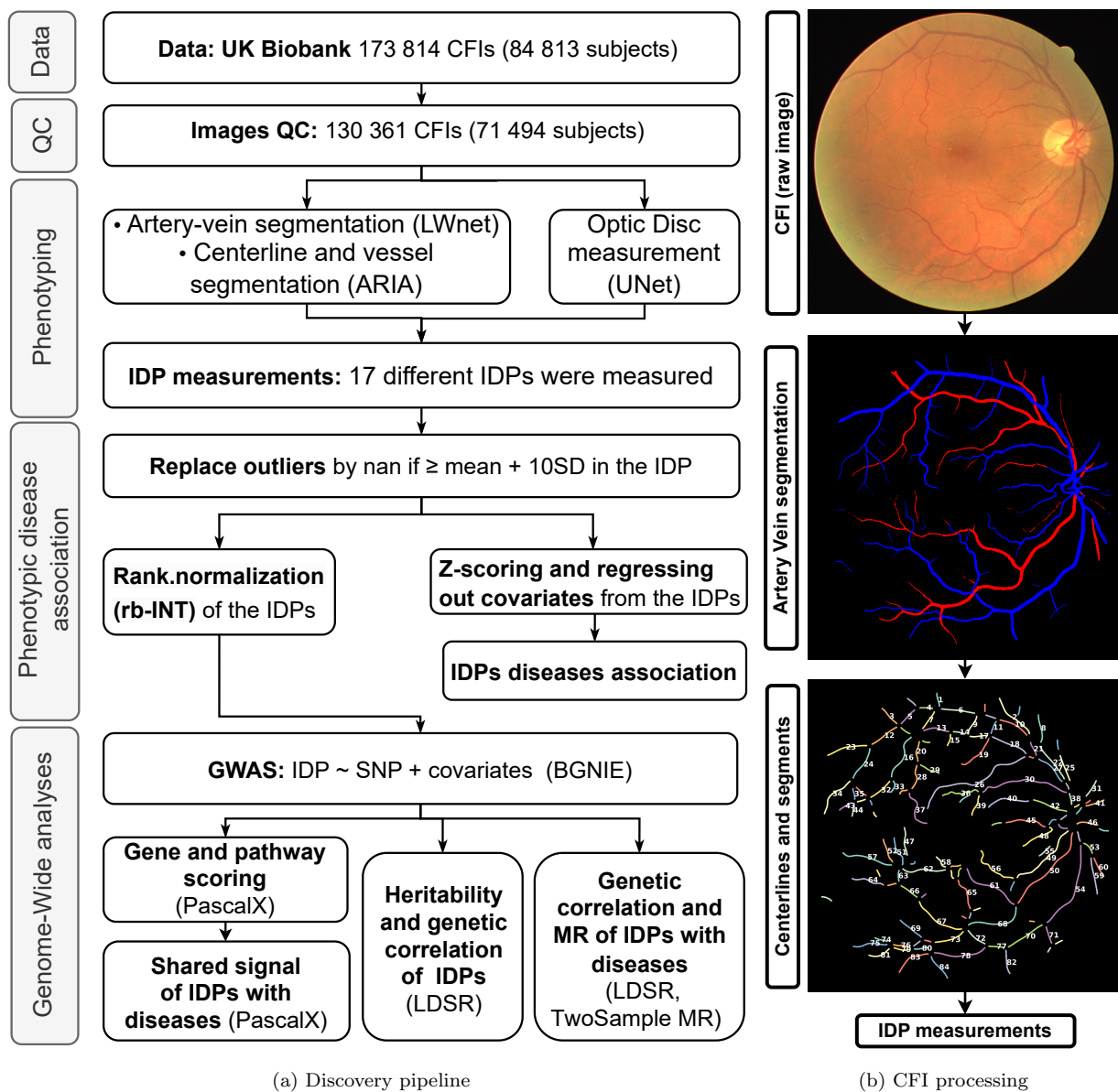


Figure 1: **a)** Overview of discovery pipeline. Subjects’ basic and medical information, genotypes, and CFIs were collected from the UKBB. Applying the Image QC method of [49] removed $\sim 25\%$ of all CFIs. Pixel-wise vessel segmentation and classification were performed using LWNET [36]. ARIA [50] was used to identify vessel segment objects. A DL network was used to measure the position of the OD [37]. Based on this primary information our bespoke algorithms measured vascular image-derived phenotypes (IDPs). IDPs (z-scored and corrected for covariates) were associated with diseases through linear and logistic regressions, and Cox models. GWAS was performed on all IDPs after rank-based inverse normal transformation (rb-INT) and correction for covariates, and the resulting summary statistics were used to estimate heritabilities and genetic correlations, to identify relevant genes and pathways, and to study the genetic association and potential causal relationships between the IDPs and some of the disease phenotypes. **b)** Overview of IDP measuring process. Top: original CFI from DRIVE dataset. Middle: Pixel-wise segmented vasculature with artery-vein classification using LWNET [36]. Bottom: Vessel segment objects in terms of centerlines and diameters were identified using ARIA [50], providing the starting point for measuring vascular IDPs (see Suppl. Text “Methods for phenotype extraction” for details).

115 Results

116 Automated pipeline for phenotyping of the retinal vasculature

117 To analyze the retinal vasculature, we developed an automated pipeline building on our previous work on
118 retinal vessel tortuosity [47]. This pipeline enabled us to segment and annotate the retinal vasculature and
119 OD from 130 361 color fundus images (CFIs) of 71 494 subjects after Quality Control (QC). We used a
120 previously established method for computing a QC score [49], and removed images in the lowest quartile of
121 this score. Applying a range of quality control thresholds, we observed that phenotype heritabilities tended to
122 be higher, while disease incident rates were lower when applying more stringent thresholds, possibly because
123 some diseases impact the vascular density which is a good proxy for image quality (see Suppl. Text “Quality
124 control threshold effect on results” for details).

125 We selected 17 representative image-derived phenotypes (IDPs) from a broader set of 36 phenotypes to
126 characterize each image, including vascular densities, median tortuosities, central retinal equivalents, median
127 diameters, diameter variabilities, and main temporal angles for arteries and veins. We also calculated the
128 ratios between artery and vein values for the first four phenotypes, and we estimated the total number of
129 vessel bifurcations. These IDPs were chosen based on their associations with diseases and the reliability of
130 measurement. The distributions of these main IDPs are presented in Suppl. Text “Distribution of retinal
131 vascular IDPs”, and their specific sample sizes in Suppl. Table “Sample size per IDP”. The broader set of
132 36 IDPs can be found in Suppl. Text “Methods for phenotype extraction”.

133 Correlation structure and heritabilities of retinal vascular IDPs

134 To explore the relationships between our main IDPs, we calculated pair-wise phenotypic Pearson correlations,
135 $r_{ij}^{(p)}$ (upper right triangle in Fig. 2a). We observed that the same IDPs measured for arteries and veins tended
136 to cluster together, in particular for the temporal angles, tortuosities, and vascular densities. Vascular
137 densities were highly correlated with each other and the number of bifurcations, the strongest correlation
138 observed. They also correlated with venous, but not arterial, tortuosity and anti-correlated with median
139 diameters. The temporal angles exhibited low correlations to the other phenotypes. Finally, most artery-
140 vein ratios were highly correlated with their corresponding arterial, and highly anti-correlated with their
141 corresponding venous measures.

142 To assess the genetic relationships between the IDPs, we estimated pair-wise genetic correlations, $r_{ij}^{(g)}$, using
143 cross-trait Linkage Disequilibrium Score Regression (LDSR) [51] (lower left triangle in Fig. 2a). On average,
144 genetic correlations were slightly higher than phenotypic correlations (standardized mean difference across
145 the 136 pairs (ij) is $d = 0.34$, $t(135)=6.53$, $p = 6.2 \times 10^{-10}$). The largest difference occurred between the
146 temporal angles. Overall there was a strong correspondence between genetic and phenotypic correlations,
147 $corr(r^{(g)}, r^{(p)}) = 0.86$, permutation $p < 1 \times 10^{-4}$ (see Suppl. Text “Correlation structure and heritabilities
148 of extended list of retinal vascular IDPs” for the corresponding analysis for our broad set of 36 IDPs and

149 Suppl. Data “Phenotypic and genetic correlations, discovery and replications” for the phenotypic and genetic
 150 correlation values of the main IDPs).

151 To gain deeper insights into the genetic control of retinal vascular morphology, we estimated the single
 152 nucleotide polymorphism (SNP) heritability, h^2 , for each IDP (Fig. 2b), using LDSR [52]. Our analy-
 153 sis revealed varying levels of heritability across our IDPs. Arterial tortuosity exhibited the highest her-
 154 itability, $h^2=0.25\pm 0.02$, followed by the tortuosity ratio, $h^2=0.20\pm 0.02$, and venous diameter variability,
 155 $h^2=0.18\pm 0.02$. In contrast, the median diameter measures, particularly arterial median diameter, showed
 156 the lowest heritability, $h^2=0.05\pm 0.01$ (see Suppl. Text “Manhattan and Quantile-Quantile plots” for Man-
 157 hattan and Quantile-Quantile plots from the GWAS of each IDP).

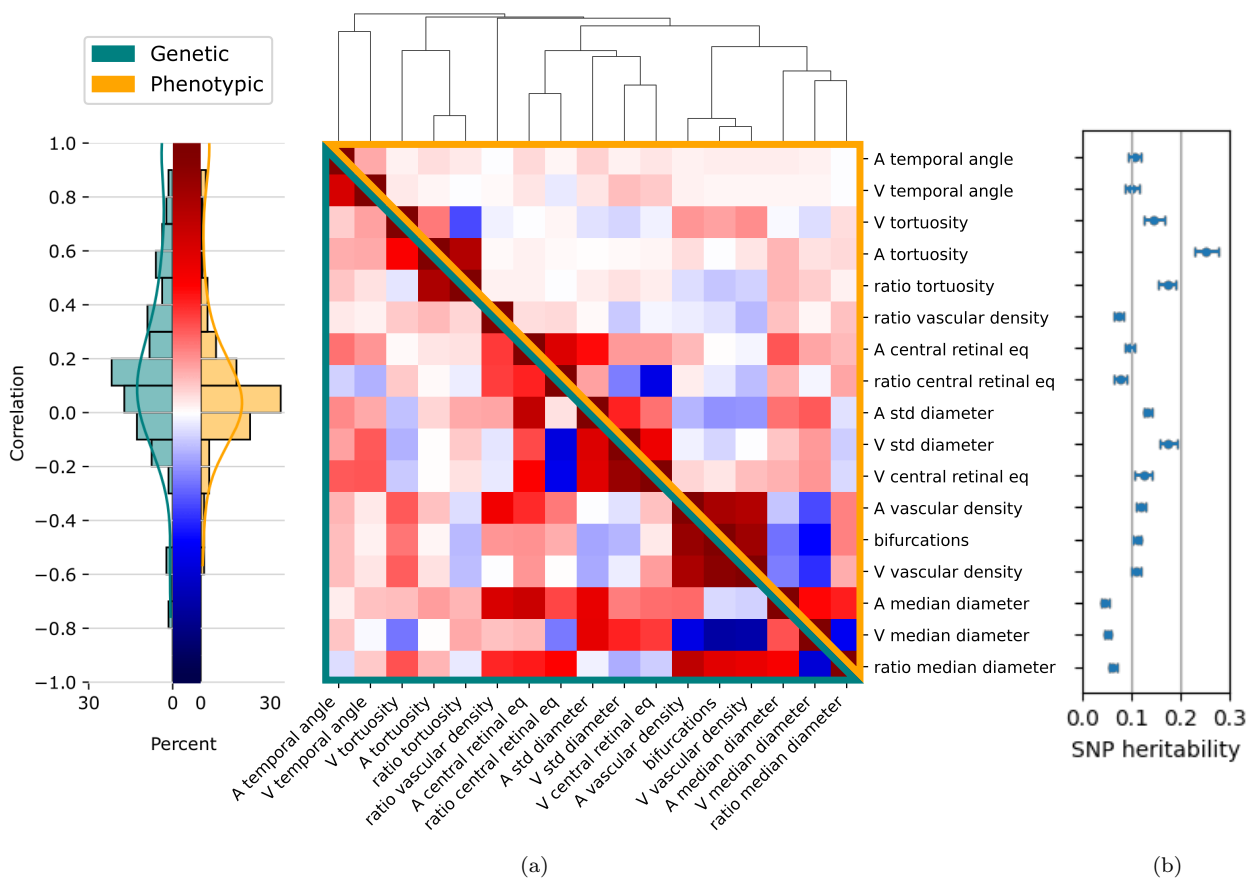


Figure 2: **a)** Phenotypic (upper-right orange triangle) and genetic (lower-left green triangle) correlations between retinal vascular phenotypes, clustered by absolute phenotypic correlation distance, $1 - |corr|$. The 17 phenotypes are (A: artery, V: vein): main temporal angles (‘A/V temporal angle’), median tortuosities and their ratio (‘A/V tortuosity’ and ‘ratio tortuosity’), central retinal equivalents and their ratio (‘A/V central retinal eq’ and ‘ratio central retinal eq’), diameter variabilities (‘A/V std diameter’), vascular densities and their ratio (‘A/V vascular density’ and ‘ratio vascular density’), median diameters and their ratio (‘A/V median diameter’ and ‘ratio median diameter’), and the number of bifurcations (‘bifurcations’). Phenotypes were corrected for age, sex, eye geometry, batch effects, and ethnicity before phenotypic clustering and before GWAS (see [Methods](#)). **b)** Corresponding phenotype SNP heritabilities, h^2 , and their standard error, estimated using LDSR [52].

158 Gene and pathway level analysis of retinal vascular IDPs

159 To identify the genes modulating specific vascular IDPs, we employed our *PascalX* analysis tool [53, 54].
160 This tool aggregates SNP-wise association signals within gene windows and generates gene scores.

161 The number of genes associated with IDPs (diagonal of Fig. 3a) ranged from 1 gene for the arterial median
162 diameter to 252 genes for arterial tortuosity. We observed the highest number of genes for tortuosities,
163 venous diameter variability, and venous central retinal equivalent. The off-diagonal elements in Fig. 3a show
164 the number of common genes for each pair of IDPs. Generally, more correlated IDPs tended to share more
165 genes. However, even among highly similar IDPs, a significant portion of genes were phenotype-specific, and
166 some IDPs shared only a few or no genes.

167 While no single gene was shared among all IDPs, two genes, *LINC00461* and *CTC-498M16.4*, were asso-
168 ciated with 9 of the 17 IDPs (Fig. 3b). Other genes associated with multiple IDPs included *SIX6*, *FLT1*,
169 *FUT1*, *HERC2*, and *PDE6G*. The complete list of significant genes associated with each IDP is available as
170 Suppl. Data “Significant genes per IDP”, and “IDP Gene scores (UKBB)”.

171 Furthermore, we conducted pathway analysis using *PascalX* to identify gene sets, or “pathways”, that
172 exhibited higher association signals for each IDP GWAS than expected by chance. Although no single
173 pathway was shared among all IDPs, some of the most frequent pathways included ‘Fetal retina fibroblast’,
174 and ‘Abnormal retinal morphology’ (Suppl. Text “Pathway analyses”). The complete list of significant
175 pathways per IDP is available as Suppl. Data “Significant pathways per IDP”.

176 To further investigate pleiotropic genes, we employed *PascalX* cross-GWAS analysis [54], a method that
177 examines coherent effects across the SNPs associated with two phenotypes within a gene window. This
178 approach has more power than just intersecting the gene sets of two individual phenotypes and also allows
179 for distinguishing between coherent and anti-coherent effects. However, even in this more sensitive analysis,
180 no single gene was shared between all pairs of phenotypes. The most pleiotropic genes largely overlapped
181 with those identified by simple gene-scoring, yet they tended to be shared among more IDPs (Fig. 3c and
182 Fig. 3d). See Suppl. Data “PascalX IDP-IDP cross gene scores” for a comprehensive list of genes. Generally,
183 IDP pairs with positive LDSR genetic correlation shared more coherent gene signals, while those with
184 negative LDSR genetic correlation had predominantly anti-coherent signals (see Suppl. Text “LDSR genetic
185 correlation against PascalX”).

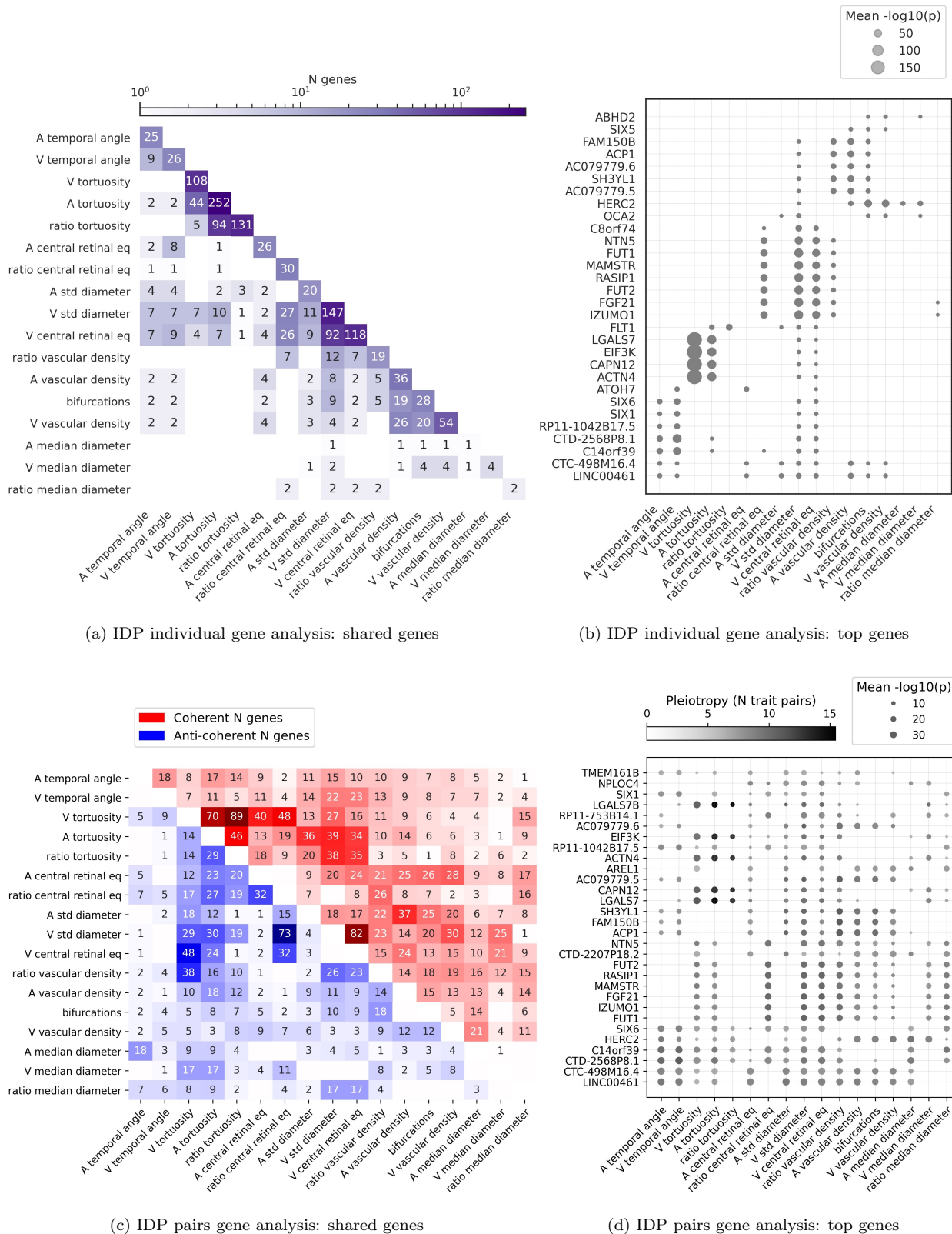


Figure 3: **a)** Number of genes associated with the different IDPs, obtained using *PascalX* gene-scoring [54]. The diagonal shows the number of genes significantly associated with each IDP. The lower triangle shows the number of genes in the intersection between pairs of IDPs. **b)** 30 genes most frequently associated with the IDPs. Dot sizes are inversely proportional to p-values. **c)** Number of genes showing coherent (top right) or anti-coherent (bottom left) signal between pairs of IDPs, obtained using *PascalX* cross-scoring [54]. **d)** 30 genes most frequently found in the cross-phenotype analysis. Dot color represents pleiotropy, i.e. the number of phenotype pairs showing (anti-)coherent signal for a given gene. Dot sizes are inversely proportional to p-values.

186 Phenotypic association with diseases and risk factors

187 To evaluate the clinical relevance of retinal vascular morphology, we examined the phenotypic associations
188 between the retinal vascular IDPs and various eye-related diseases, vascular diseases, and their associated
189 risk factors. We employed linear regression for continuous diseases variables (that correspond to risk factors)
190 (Fig. 4a), logistic regression for binary disease states (Fig. 4b), and Cox models for diagnoses with age-of-
191 onset (Fig. 4c). All IDPs were standardized (z-scored) and adjusted for potential confounders.

192 Amongst the risk factors, diastolic blood pressure (DBP) and systolic blood pressure (SBP) displayed similar
193 associations with most IDPs. Smoking pack-years exhibited the strongest positive association with venous
194 diameter variability, $\beta = 0.12$, while the strongest negative correlations were observed between blood pressure
195 (BP) and arterial-related IDPs, particularly the central retinal equivalent, vascular density, and median
196 diameter $\beta \in [-0.18, -0.13]$ (Fig. 4a).

197 For binary disease states, hypertension was positively associated with venous tortuosity and less with arterial
198 tortuosity, while negatively associated with central retinal artery equivalent, and the ratios of central retinal
199 equivalents and vascular densities, among others. Eye diseases such as amblyopia were negatively associated
200 with the number of bifurcations and venous vascular density, $\beta \approx -0.16$. Others like presbyopia, hyperme-
201 tropia, and myopia showed smaller effects, $\beta \in [-0.08, 0.06]$, but were still statistically significant. Retinal
202 diabetes was negatively associated with the vascular densities and the number of bifurcations, $\beta \in [-0.30,$
203 $-0.25]$, while atherosclerosis was positively associated with venous diameter variability, $\beta = 0.34$ (Fig. 4b).

204 The Cox model analysis for age-of-onset phenotypes included severe eye- and cardiovascular diseases, dia-
205 betes, and age at death. Both vascular densities displayed consistent associations with the age of diagnosis
206 for all eye-related diseases. Diabetes age-at-diagnosis shared similar associations with our vascular IDPs
207 as retinal diabetes, but was also associated with venous tortuosity and central retinal arterial equivalent,
208 among others. Heart attack was associated with larger median arterial diameter and central retinal arte-
209 rial equivalent, as well as diameter variability in both vessel types. Importantly, earlier deaths were most
210 strongly associated with increased venous diameter variability and less strongly with increased central venous
211 retinal equivalent, increased venous temporal angles, decreased vascular density, and fewer bifurcations. In
212 general, venous diameter variability was associated with almost all diseases, including the only associations
213 with pulmonary embolism and stroke (Fig. 4c). For a complete table of the standardized effect sizes, hazard
214 ratios and p-values, see Suppl. Data “IDPs phenotypic association with diseases”.

215 While the vascular densities and the number of bifurcations were highly inter-correlated, their associations
216 with diseases sometimes differed. For instance, SBP and hypertension were associated with arterial vascular
217 density and the number of bifurcations but not with venous vascular density. An equivalent analysis of 17
218 leading principal components (PCs) of our IDPs revealed no novel or stronger disease associations compared
219 to the raw IDPs (see Suppl. Text “Principal Component Analysis”).

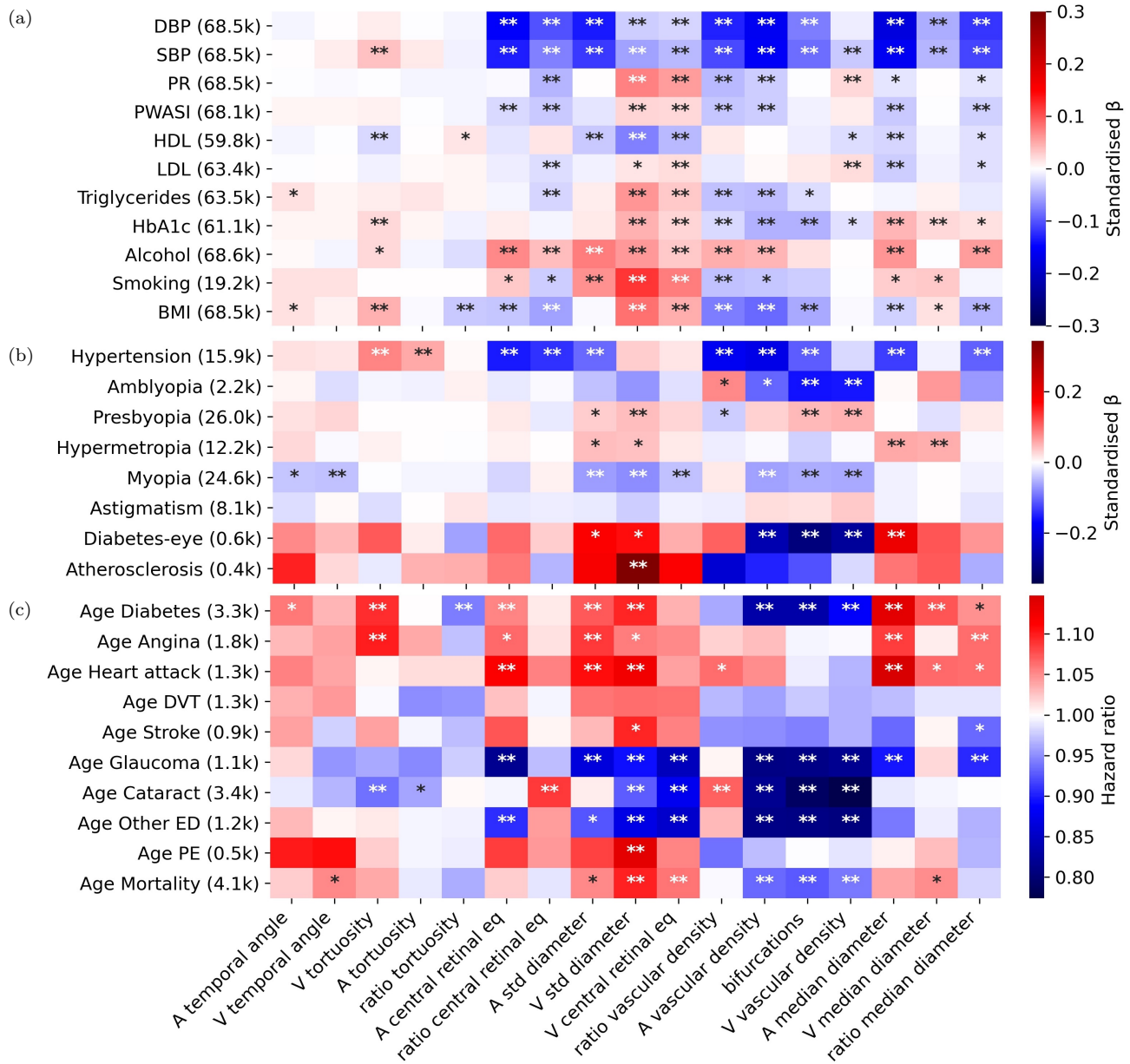


Figure 4: Phenotypic association of IDPs with risk factors and diseases. The x-axis shows IDPs and the y-axis shows risk factors and diseases. The numbers in parentheses correspond to the number of subjects with this information for which we were able to measure at least one of the 17 IDPs, for continuous diseases. For binary disease states, it represents the number of subjects who were cases and had data for at least one of the 17 IDPs. Linear (a) and logistic (b) regressions were used for continuous and binary disease states, respectively. For age-of-death and other severe diseases with the age-of-onset information, Cox proportional hazards regression was performed (c). In all models, phenotypes were corrected for age, sex, eye geometry, batch effects, and ethnicity. The color indicates standardized effect sizes for linear and logistic regressions or hazard ratios for Cox models. Asterisks indicate the level of statistical significance (* : $p < 0.05/N_{tests}$, ** : $p < 0.001/N_{tests}$, where $N_{tests} = N_{IDPs} \times N_{traits}$, and N_{traits} is the number of diseases or risk traits considered in each panel). Labels: ‘PR’: Pulse rate, ‘PWASI’: Pulse wave arterial stiffness index, ‘HDL’: High-density lipoprotein, ‘LDL’: Low-density lipoprotein, ‘HbA1c’: Glycated hemoglobin, ‘Alcohol’: Alcohol intake frequency, ‘Smoking’: pack-years, ‘BMI’: Body mass index, ‘Diabetes-eye’: Diabetes related to the eye, ‘DVT’: Deep vein thrombosis, ‘Other ED’: all types of severe eye diseases not included explicitly, ‘PE’: Pulmonary embolism.

220 Genetic associations with diseases and causality analysis

221 To investigate the extent of common genetic architectures between the vascular IDPs and risk factors, we
222 first used LDSR to estimate their genetic cross-correlations. Notably, we observed the strongest negative
223 correlations (≈ -0.30) between BP measures and the ratios of the central retinal equivalents, and vascular
224 densities. Body mass index (BMI) was correlated positively with median vein diameter (≈ 0.15), and its
225 variation (≈ 0.18), and negatively with arterial vascular density and the number of bifurcations (Fig. 5a).
226 HbA1c was also negatively correlated with the number of bifurcations, while HDL was negatively correlated
227 with venous diameter variability, but only with marginal significance. For binary disease states, we found
228 weaker associations; however, hypertension exhibited associations similar to those of blood pressure. For
229 further details on binary disease states, see Suppl. Text “Genetics associations between vascular IDPs and
230 binary diseases”.

231 To compare the phenotypic and genetic associations between vascular IDPs and risk factors, we plotted the
232 effect sizes of the phenotypic linear regressions against genetic correlations for each IDP/risk factor pair
233 (Fig. 5b). The slopes of the best-fitting lines through the corresponding points were positive for all risk
234 factors, except for LDL cholesterol.

235 A strong genetic association between two phenotypes does not imply the existence of a causal link. To
236 systematically assess potential causal relationships between vascular IDPs and risk factors, we performed
237 bidirectional two-sample Mendelian Randomisation (MR) analyses [55, 56]. Causal estimates were derived
238 from the inverse variance weighted method using the TwoSampleMR R package [57, 58]. We used false
239 discovery rate (FDR) to correct for multiple testing and we also performed sensitivity analyses that confirmed
240 the robustness of our results (see Methods and Suppl. Data “MR risk factors (IVW)” for complete results).

241 Using risk factors as exposures, we observed evidence for causal effects on most of the IDPs, even after
242 adjusting for multiple testing (see Fig. 5c). Notably, we found strong evidence for negative effects of DBP
243 and SBP on many different vascular IDPs, including arterial (and ratio) central retinal equivalent, arterial
244 (and ratio) median diameter, vascular density and bifurcations. Also, SBP had a positive effect on arterial
245 and venous tortuosity. BMI had a positive effect on venous (and arterial) diameter variability and venous
246 central retinal equivalent, while it showed a negative effect on ratio central equivalent, ratio vascular density
247 and bifurcations. Furthermore, alcohol intake had a positive effect on arterial (but not venous) diameter
248 variability, while HbA1c levels had a weak negative effect on arterial vascular density, bifurcations and arterial
249 diameter variability. We also observed other potential causal effects, but only with marginal significance
250 ($p_{uncorrected} < 0.05$). For example, PR had a positive effect on venous diameter variability and a negative
251 effect on arterial temporal angle, while LDL levels had a positive effect on arterial tortuosity and ratio central
252 equivalent.

253 In contrast, using IDPs as exposures, only the causal effect of ratio central equivalent on BP (SBP and DPB)
254 survived FDR correction. We also observed potential causal effects on risk factors for many other vascular

255 traits, but only with marginal significance ($p_{uncorrected} < 0.05$) (see Fig. 5d). For example, we identified
 256 arterial tortuosity and venous diameter variability as positive causal factors for BP, while the ratio of central
 257 equivalent had a negative effect on BP. Venous diameter variability (and venous median diameter) also had
 258 a negative effect on HDL levels, while arterial median diameter had a positive effect on PR. Significant
 259 causal effects were also found between vascular IDPs and binary disease states; see Suppl. Text “Mendelian
 260 Randomization analysis between vascular IDPs and binary diseases”.

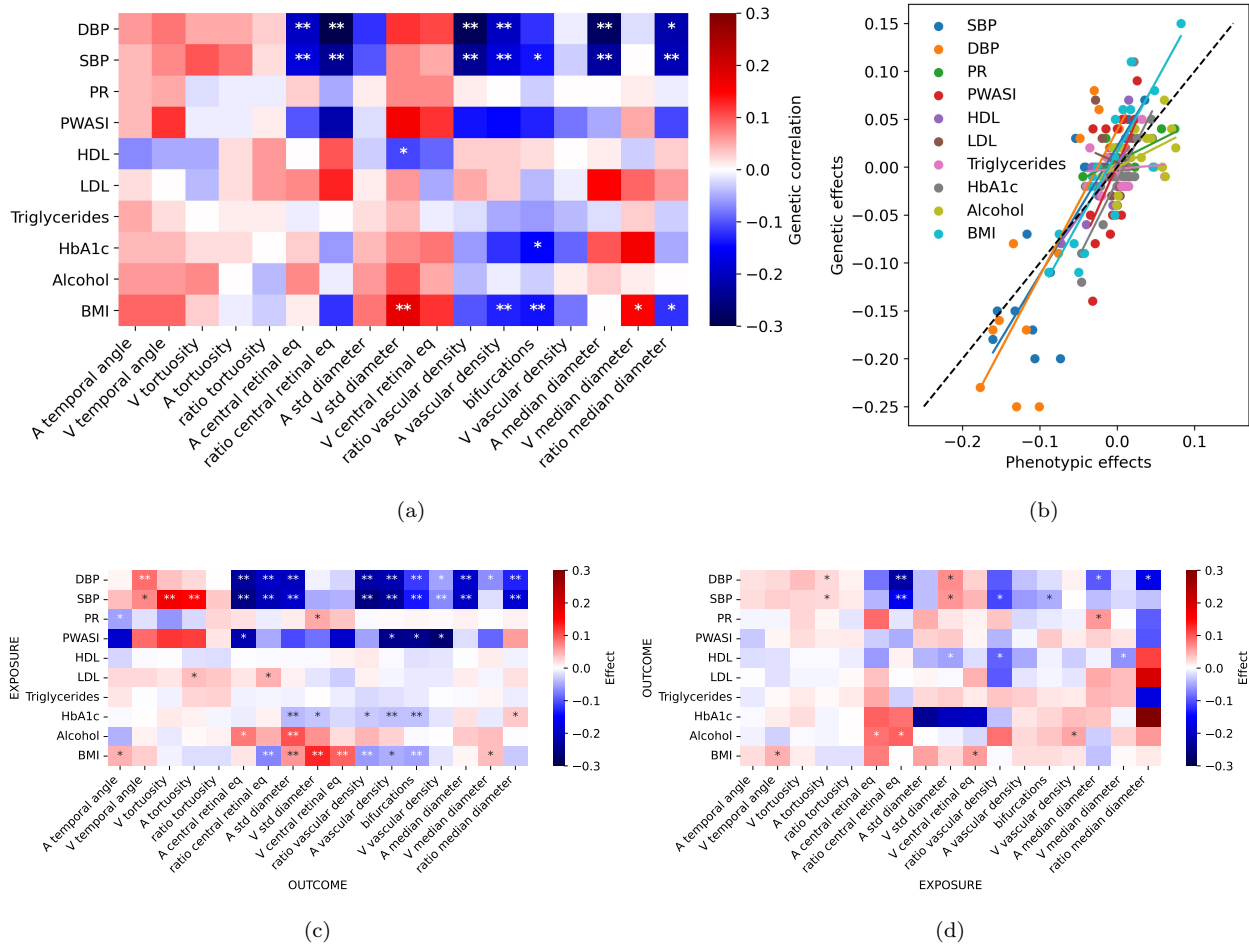


Figure 5: **a)** Genetic correlation between IDPs and risk factors, computed using LDSR [52]. The color indicates the genetic correlation coefficient and the asterisks indicate the level of statistical significance ($* : p < 0.05/N_{test}$, $** : p < 0.001/N_{test}$, being $N_{test} = N_{IDPs} \times N_{LinearDiseases}$). **b)** Correlation between phenotypic and genetic correlations of IDPs with risk factors. **c)** Causal effect estimates with risk factors as exposures and IDPs as outcomes. **d)** Causal effect estimates with IDPs as exposures and risk factors as outcomes. The color indicates the causal effect estimates based on the inverse variance-weighted MR method. The level of statistical significance is indicated with a single asterisk for nominal significance without correction for multiple testing ($* : p_{uncorrected} < 0.05$) and two asterisks for a FDR ($** : p_{FDR} < 0.05$).

261 In order to identify genes that were jointly associated with IDPs and risk factors, we first computed simple
 262 intersections between the corresponding gene sets of such pairs (Fig. 6a). This revealed some sizable overlaps,
 263 in particular for vein diameter variability and central equivalent with BP measures, triglycerides, HbA1c,

264 and BMI. Applying *PascalX* cross-GWAS analysis [54], as previously for the pairs of two vascular IDPs,
265 we were able to identify many new candidates for pleiotropic genes (Fig. 6b and 6c). We observed that
266 the sets of coherent genes (Fig. 6b) tended to be largest for phenotype pairs whose sets of associated genes
267 already had a sizable overlap, while we found large sets of anti-coherent genes (Fig. 6c) for some phenotype
268 pairs whose associated genes had no or only little overlap, notably for DBP and the ratio of the central
269 retinal equivalents, the ratio of the vascular densities and the median arterial diameter and its variability.
270 Moreover, the ratio of central retinal equivalents shared multiple anti-coherent genes with BP and BMI
271 (see Suppl. Data “[PascalX IDP-disease cross gene scores](#)” for a comprehensive list of genes). For a similar
272 analysis for binary disease states, we found weaker associations; however, hypertension exhibited associations
273 similar to those of blood pressure. For further details on binary disease states, see Suppl. Text “Genetics
274 associations between vascular IDPs and binary diseases”.

275 Shared pathways between the IDPs and diseases can be found in the Suppl. Text “Pathway analyses between
276 vascular IDPs and diseases”.

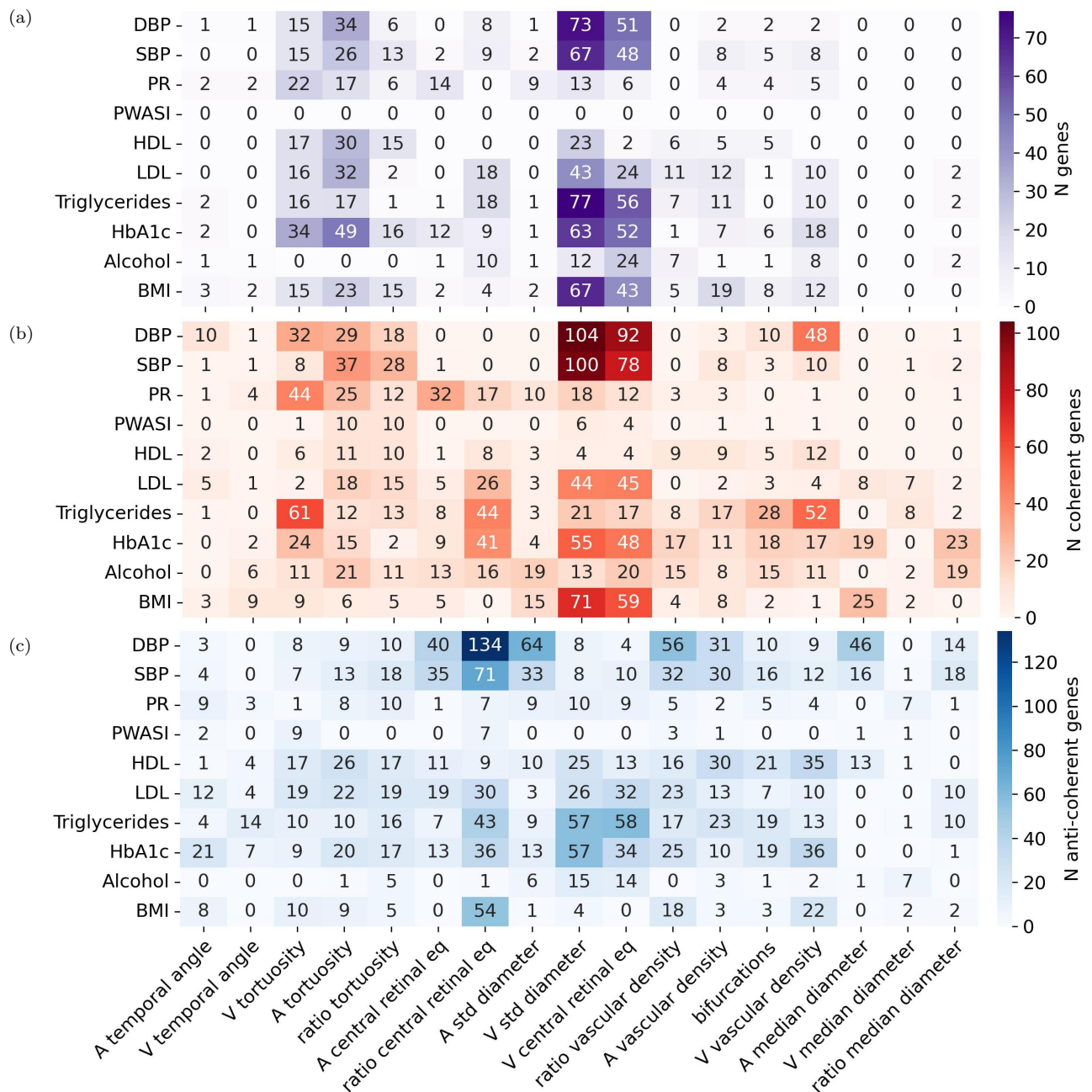


Figure 6: **a)** Gene-scoring plain intersection showing genes in common between IDPs and risk factors. Each cell shows the number of intersected genes in phenotype pairs. **b)** and **c)** Cross-phenotype coherence analysis showing the number of coherent **b)** and anti-coherent **c)** genes between phenotype pairs. Summary statistics for risk factors were obtained from <http://www.nealelab.is/uk-biobank>, and gene-level analyses were computed using *PascalX* [54].

277 Replication analysis

278 We had access to CFIs from two independent smaller cohorts, namely the Rotterdam Study (RS, N=8 142
 279 participants) and OphtalmoLaus (N=2 276 participants), from which we computed our 17 IDPs. While we
 280 used an identical analysis pipeline for OphtalmoLaus, a novel annotation software was developed for the RS

281 images, adapted to their specifics, notably including a dedicated and internally validated vessel segmentation
282 tool (“VascX”, manuscript in preparation). Phenotypic correlations $r_{ij}^{(p)}$ between IDPs obtained in the two
283 replication cohorts were globally concordant with those from the UKBB data ($\rho=0.86$, $p=7.5 \times 10^{-42}$ for
284 OphthalmoLaus and $\rho=0.69$, $p=1.8 \times 10^{-20}$ for RS, see Fig. 7a). Notably, we replicated the high phenotypic
285 correlation between vascular densities and the number of bifurcations and the low correlation between the
286 temporal angles and the other IDPs. The main difference was that for RS data we observed a positive
287 correlation between the variability in arterial diameter and vascular densities, while it was negative for
288 UKBB and OphthalmoLaus (see Suppl. Text “IDPs phenotypic replication” for details), which may be due
289 to the different vessel segmentation tool used for RS images. We also observed many consistent associations
290 between IDPs and disease traits in the RS (when available, see Suppl. Text “IDPs phenotypic replication”
291 for details).

292 Because of its larger sample size we used exclusively RS data to attempt replication of our genetic associations
293 results in the UKBB. Since RS consists of four sub-studies with different sample sizes (RS-I: 2 391, RS-II: 877
294 RS-III: 2 811, and RS-IV: 2 063 participants) GWAS were performed independently for each of them, and
295 then meta-analysed (see Suppl. Text “IDPs genetic replication” for the corresponding Manhattan and QQ-
296 plots). Applying LDSR to estimate IDP SNP heritabilities and genetic cross-trait correlations, we observed
297 overall consistency with the estimates from the UKBB data ($\rho=0.74$, $p=0.001$ for the former and $\rho=0.45$,
298 $p=5.63 \times 10^{-12}$ for the latter, see Fig. 7b and c). Notably, in RS arterial tortuosity ($h^2=0.22\pm 0.07$), the
299 tortuosity ratio ($h^2=0.20\pm 0.06$) and variability in venous diameter ($h^2=0.18\pm 0.06$) also had the highest
300 heritability estimates. Plotting the effect sizes for significant SNPs in the UKBB against those of the
301 RS (Fig. 7d) revealed highly significant correlations and concordance in direction for the vast majority
302 of IDPs. We then sought to replicate individual genetic associations. To this end, we applied the well-
303 established Benjamini-Hochberg procedure [59]. With a fixed FDR of 0.05, we replicated 86 SNPs out of
304 195 across the four IDPs shown in Fig. 7e, and 232 SNPs out of 566 were replicated across the 17 main IDPs
305 (see Suppl. Text “IDPs genetic replication”). The complete figure with all the 17 IDPs and the RS SNP
306 heritabilities can be found in Suppl. Text “IDPs genetic replication”.

307 Finally, to identify the genes modulating specific vascular IDPs in the replication cohort (RS), we employed
308 our *PascalX* analysis tool [53, 54]. We applied the Benjamini-Hochberg procedure [59] for the genes. With a
309 fixed FDR of 0.05, we replicated 93 genes out of 310 across the four IDPs shown in Fig. 7f. The complete set
310 of RS gene scores can be found in the Suppl. Data “IDP Gene scores (RS)” and a table with genes associated
311 with each RS IDP can be found in Suppl. Text “IDPs genetic replication”. For a more detailed explanation
312 of the SNPs and genes replication using the Bonferroni threshold as discovery and the Benjamini-Hochberg
313 procedure as replication, see Suppl. Data “SNPs replication: UKBB replicated in RS, and RS replicated in
314 UKBB”, and “Genes replication: UKBB replicated in RS, and RS replicated in UKBB”.

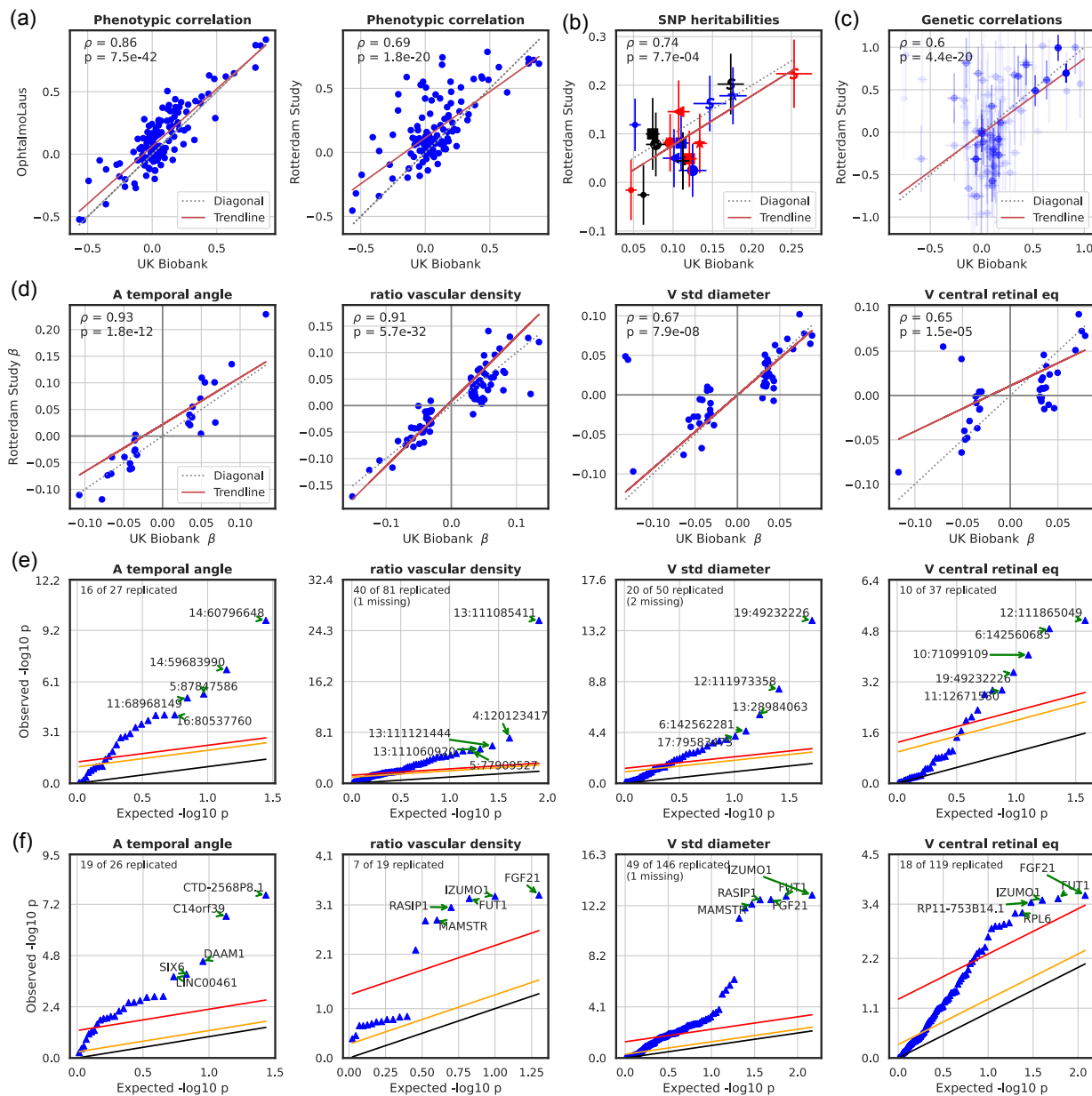


Figure 7: **a)** Scatter plot of the phenotypic correlations between our 17 IDPs in the UKBB and in the replication cohorts, OphtalmoLaus (left) and RS (right). IDPs were corrected for age, sex, eye geometry, and ethnicity (see [Methods](#)). **b)** Correlation of SNP heritabilities, using LDSR, between our 17 IDPs in the discovery (UKBB) and the replication cohort (RS). **c)** Scatter plot of the genetic correlations, using LDSR, between our 17 IDPs in the discovery (UKBB) and the replication cohort (RS). Weighted-least square regression was used to determine trendline and the significance of the association. To distinguish between the different IDPs, the following color and shape legend was utilized: ‘S’ denoted tortuosity, ‘*’ for standard deviations, ‘<’ for temporal angles, the ‘<’ for bifurcations, and ‘□’ for vascular density. While the red color is used for arteries, blue for veins, and black for no specific vessel type. **d)** Correlation of effect sizes at the SNP level in the discovery (UKBB) and the replication cohort (RS). **e)** Benjamini-Hochberg procedure on discovery lead SNPs from the UKBB using the RS. FDR = 0.05 in red, FDR = 0.5 in orange, and observed = expected line in black. The label “missing” indicates that these SNPs were not available in the replication cohort. **f)** Benjamini-Hochberg procedure on genes discovered in the UKBB using the RS. The color code is the same as in the previous subfigure. The complete figures can be found in Suppl. Text “IDPs genetic replication”.

315 Discussion

316 In this study, we established an automated analysis pipeline to extract 17 retinal vascular phenotypes from
317 CFIs and applied it to over 130k CFIs of close to 72k UKBB subjects. While some of these phenotypes had
318 previously been studied individually, our work is the first to provide a common reference. Our phenotyping
319 procedure, automated and open access, enabled us to study jointly a large panel of retinal vascular pheno-
320 types, some of which (temporal angles, central equivalents, number of bifurcations) were assessed for the first
321 time in a large cohort. We provided a comparison of the phenotypic with genotypic correlation structures
322 of these IDPs. We estimated their heritabilities, and elucidated associated genes and pathways, allowing us
323 to identify common and disjoint genetic architectures. We studied associations of our IDPs with a spectrum
324 of diseases and risk factors providing evidence of their complementarity for indicating specific disease risks.
325 For validation, we reproduced the phenotypic correlation structure in two independent cohorts, the RS and
326 OphthalmoLaus, with 8.1k and 2.2k participants respectively, and validated numerous GWAS results in the
327 RS. Importantly, the RS analysis pipeline was coded independently (to adapt to the specifics of their CFIs),
328 such that these successful replication results provide strong evidence that our phenotyping is robust and not
329 driven by cohort specific effects.

330 The phenotypic correlations revealed distinct clusters of vascular IDPs. One cluster includes vascular arterial
331 and venous density, previously linked to fractal dimension [49], and the number of bifurcations. Our results,
332 both the discovery and replications, suggest that the number of bifurcations, which is challenging to identify,
333 can be reliably estimated using vascular densities. Interestingly, diameter variabilities showed stronger
334 correlations with central retinal equivalents (of the same vessel type) than with the median diameters,
335 suggesting that larger vessels dominate diameter variability. Indeed, median diameters (especially for veins)
336 are confounded by vascular density, which is probably due to CFIs with lower vascular density exhibiting
337 less blood vessels of small caliber. The latter may be due to degeneration of the vasculature, but also to
338 poorer image quality, in particular blurriness, which is impacted by corneal opacity. More work is needed to
339 disentangle the different distributions to establish robust diameter measures for blood vessels not proximal
340 to the OD. Finally, the temporal angles exhibited little correlation with other vascular IDPs, both in the
341 discovery and replication cohorts, indicating that they may be influenced by non-vascular factors, such as
342 eye anatomy.

343 The genetic correlation between IDPs largely mirrored their phenotypic correlation, supporting Cheverud's
344 conjecture which states that phenotypic correlation can be used as a proxy for genetic correlation [60].
345 However, in our study genetic correlations were slightly larger on average, indicating potential differential
346 effects of environmental factors on correlated IDPs.

347 We observed significant variation in heritability estimates among different vascular IDPs. Tortuosity and
348 vascular density showed comparatively high heritability, consistent with some previous findings [47, 49]. A
349 recent study [48] estimated heritability of retinal arteriolar tortuosity at 0.51 using UKBB data, substan-

350 tially higher than our 0.25 estimate. Our point estimate in the RS is 0.22 ± 0.07 , which is consistent with
351 our estimate from UKBB data. We note that here we used median tortuosity across all vessel segments
352 independent of their caliber and length, even though tortuosity may vary as a function of blood vessel length
353 and diameter, calling for more refined or stratified measures.

354 Notably, venous diameter variability also exhibited high heritability, which may be partially attributed to
355 vascular beading, severe forms of which are known to be inherited [61]. Interestingly, the heritability of
356 temporal angles was relatively low, likely reflecting sensitivity to environmental factors, as well as measure-
357 ment noise and methodological variations, such as variability in the position of the OD across images, and
358 variation due to refraction that may be insufficiently corrected by spherical and cylindrical power as our
359 covariates. Future work could use heritability as a guide for developing more robust measures of these angles
360 both in terms of the methodology for extracting them (see Suppl. Text “Methods for phenotype extraction”
361 for our procedure) and implementing proper corrections for potential confounders. Finally, median vessel
362 diameters obtained the smallest heritabilities, consistent with their known dependence on the environment,
363 such as vasoconstriction induced by stress, and diseases, as well as the aforementioned confounding by image
364 quality and age-dependent reduction in detectable small blood vessels.

365 Gene analysis of individual IDPs replicated some previously identified gene associations with explicit vascular
366 phenotypes, namely tortuosity [46–48], fractal dimension, vascular density [49], and vessel width [48], as well
367 as DL vascular phenotypes representing the latent space of an autoencoder [39] (see Suppl. Text “Comparison
368 with previous GWAS” for complete list). Diameter variability and central retinal equivalent, particularly for
369 veins, received numerous gene associations, providing evidence for the genetic complexity of these phenotypes.
370 Finally, the ratios of vascular measures, combining arterial and venous components, showed associations
371 with genes not found in individual measures, indicating sensitivity to vessel-type specific effects. Generally,
372 phenotypes with higher heritability tended to have more associated genes, with some exceptions like arterial
373 diameter variability.

374 No single gene was significantly associated with all the vascular IDPs. The most frequently observed gene
375 was *LINC00461*, also known as visual cortex-expressed gene (VISC), an evolutionarily conserved long non-
376 coding RNA that produces several alternatively spliced transcripts [62]. Other frequently observed genes are
377 related to eye diseases (*PDE6G* has been linked to Retinitis Pigmentosa, and *SIX6* to glaucoma, myopia,
378 and retinal degeneration) or vascular processes (*FLT1* linked to hypertension and heart disease). Also,
379 *HERC2* and *OCA2*, two neighboring genes related to pigmentation, were linked to multiple IDPs. *OCA2* is
380 involved in the production of melanosomes, and therefore directly contributes to the formation of pigments,
381 while mutations in *HERC2* have been found to modulate *OCA2* expression [63]. We speculate that less
382 eye pigmentation leads to reduced protection from damaging light, which could cause global changes on the
383 retinal surface, including vascular morphology.

384 Our study of phenotypic associations between vascular IDPs and disease-relevant phenotypes confirmed
385 some previously known associations, such as the link between vessel diameter and hypertension, likely due

386 to alterations in vascular resistance and blood flow [3, 4, 64]. Interestingly our MR analysis provides sup-
387 port for a low ratio of the central retinal equivalent being causal for high BP. This is consistent with a
388 positive (but not significant) phenotypic and genetic correlation between central retinal venular equivalent
389 and hypertension/BP. We also observed significant associations between IDPs capturing arterial vessel cal-
390 iber and heart attack, consistent with previous findings [18, 43–45, 65, 66], and the previously observed
391 link between tortuosity and cardiovascular risk factors [10, 67]. For a more complete discussion refer to
392 Suppl. Text “Replication of previously identified associations of retinal vascular phenotypes with diseases”.
393 Additionally, we found diameter variability in both vessel types to be positively associated with heart attack,
394 possibly due to the formation of plaques that enlarge the vessel while reducing lumen diameter and negatively
395 impacting blood flow. While atherosclerosis has a similar association profile across the vascular phenotypes,
396 interestingly the association with venous diameter variability was the strongest and the only one passing
397 statistical significance. This signal may be driven by artery-vein crossings and calls for further investigation.

398 Type-2 diabetes is known to affect the microvascular circulation in the retina resulting in a range of structural
399 changes unique to this tissue, such as neovascularization [68], which can affect vascular density [49] and
400 arteriolar tortuosity [69], among others. We note that the association profile of our IDPs with HbA1c,
401 which is used to diagnose type-2 diabetes [70], is similar, but typically a bit weaker in terms of effect size and
402 significance than the latter, suggesting that our Cox model taking into account the age of onset of the disease
403 endpoint has more power. Given that diabetes is a known risk factor for cardiovascular disease, including
404 angina, this could explain why many associations between type-2 diabetes and IDPs related to vessel caliber
405 are also observed for angina and heart attack.

406 Age at death is the only trait, besides myopia, that is associated with the venous temporal angle. Moreover,
407 age at death also shares some of the associations of specific diseases with our IDPs, such as a negative
408 association with the number of bifurcations (in line with the results for hypertension and type-2 diabetes
409 reported above), and positive associations with several vein-related phenotypes besides the temporal angle,
410 including the diameter variability, the median diameter (in line with the results for stroke, type-2 diabetes,
411 heart attack and atherosclerosis reported above). It seems plausible that the reduced lifespan for these
412 common diseases explains the observed associations.

413 MR analysis allowed assessment of potential causal directions for the links observed in the correlation analy-
414 sis. Overall the effects of CVD risk factors on our vascular IDPs tend to be stronger and more significant than
415 the reverse, underlining the usefulness of IDPs for early diagnosis of CVD. Consistent with previous findings,
416 we found that individuals with genetically elevated BP tend to have lower retinal vascular density [49]. In
417 addition, we found several other IDPs being affected, suggesting that vascular remodeling can be caused by
418 elevated BP. Also, elevated BMI may cause higher variability in venous and arterial diameter, consistent
419 with the finding that obesity may decrease venous return of blood from the lower extremities thereby in-
420 creasing the risk of chronic venous insufficiency [71]. Amongst the strongest potential reverse causal effects
421 is the aforementioned decrease in BP due to a higher ratio of the central retinal equivalent. Additionally, we

422 found that higher arterial tortuosity tends to increase BP, confirming previous findings [48]. Interestingly, we
423 also found that vein diameter variability may also cause higher BP, which could be mediated by anatomical
424 alterations such as venous beading. However, those findings were not significant after correcting for multiple
425 testing. The recent paper by Jiang et al. [48] also reported a causal effect of arterial tortuosity on Coronary
426 Heart Disease (CHD). We were able to confirm this causal link of arterial tortuosity on CHD, while no other
427 retinal trait was found to be causal (see Suppl. Text “Mendelian Randomization analysis between vascular
428 IDPs and binary diseases”).

429 In the gene analysis, we observed that the pairs of diseases and IDPs with the highest positive correlations
430 tended to have a greater number of shared genes, both in the intersection and coherence analyses (see
431 Suppl. Text “LDSR genetic correlation against PascalX”). It is worth noting that this was not limited to
432 pairs with high-significance values. Besides, we again observed that the patterns differed in the analysis
433 of coherent and anti-coherent genes. For example, vein diameter variability and BMI had multiple genes
434 associated coherently, implying that the genes modulating them acted in the same direction. Conversely,
435 between BMI and the central equivalent ratio, the majority of genetic effects acted in the opposite direction.
436 This is consistent with the previous finding that vein diameter variability and ratio central equivalent shared
437 many anti-coherent genes.

438 While our study pushes the boundaries of analysing retinal vascular phenotypes, it has several important
439 limitations: First, limiting our study to data from the UKBB, RS, and OphthalmoLaus makes our findings
440 specific to a population of mostly European ancestry. Second, there are some other potentially relevant
441 vascular IDPs that we did not analyze, including branching angles, artery-vein crossings, and neovascular-
442 ization. Third, our GWAS did not include the analysis of sex chromosomes or rare variants. The exclusion
443 of these factors may have limited the scope of the study and prevented the identification of potential associ-
444 ations between genetic variations and the development of certain diseases or phenotypes. Finally, summary
445 statistics used for the genetic analysis of binary disease states were not obtained using GWAS with logistic
446 regression, but linear regression, which can have an effect a sensitivity effect on their results (see methods:
447 [Genetic association with diseases](#)).

448 In summary, this study establishes a common framework for studying multiple vascular phenotypes of the
449 retina. The explicit characterisation of retinal vasculatures will be useful both for clinical research further
450 exploring their usefulness as biomarkers for systemic diseases, and fundamental research, where we provide
451 an important alternative reference to implicit characterizations of the retina, such as the recent “Foundation
452 model” for retinal images [40]. Our analysis of genes and pathways unveiled a strikingly limited intersection,
453 indicating that the mechanisms governing these phenotypes are largely independent. Our findings regarding
454 the association between disease phenotypes affirmed some established knowledge while uncovering numerous
455 novel connections. Specifically, we observed a plethora of intriguing new links between diameter variability,
456 particularly in veins, and various disease phenotypes such as age of mortality, pulmonary embolism, and
457 myocardial infarction. While more work is needed to further validate and extend our findings, our analyses

458 provide evidence that we start to have sufficient power for obtaining functional, as well as some initial causal
459 insights into the genetic and disease-related processes modulating the retinal vasculature.

460 **Methods**

461 **UK Biobank data**

462 The UKBB is a population-based cohort of approximately 488k subjects with rich, longitudinal phenotypic
463 data including a complete medical history, and a median 10-year follow-up [72, 73]. Standard retinal 45° CFIs
464 were captured using a Topcon Triton 3D OCT 1000. 173 814 images from 84 813 individuals, were analyzed.
465 Genotyping was performed on Axiom arrays for a total of 805 426 markers, from which approximately
466 96 million genotypes were imputed. We used the subset of 15 599 830 SNPs that had been assigned a
467 rsID. Baseline and disease information about the subjects whose images were analyzed can be found in
468 Suppl. Text “Baseline characteristics”.

469 **Image segmentation and quality control**

470 Raw CFIs were segmented into pixel-wise segmentations of arteries and veins using the DL model LWNET [36],
471 which had been trained on the publicly available DRIVE dataset. To detect the OD, a random set of 100
472 CFIs of varying quality from the UKBB were first annotated, and the resulting ground truths were then
473 used to retrain a standard U-Net previously trained to detect the OD in various public datasets [37]. Last,
474 branch points of vessels and vessel-segment-wise and centerlines were extracted using skeletonization, and
475 diameters were extracted using the distance transform, both provided in ARIA [50].

476 A published QC method [49] to assess image quality in the UKBB was used, and the 75% highest-quality
477 CFIs according to this method were retained for further analysis. In this method, the image quality of 1 000
478 CFIs was quantified by professional graders, and a CNN was then trained to imitate the graders’ quality
479 assessment. A significant negative correlation between image quality and age was observed, $r=-0.21$, but
480 was not corrected. For more information refer to Suppl. Text “Image segmentation”. Additionally, to see
481 how the threshold on the QC can affect the results refer to Suppl. Text “Quality control threshold effect on
482 results”.

483 **Phenotyping**

484 Retinal vessel morphology was broadly phenotyped, drawing on a set of known relevant ophthalmological
485 phenotypes, including a few that were previously undescribed, such as diameter variability. Due to the lack
486 of consensus definitions and methods for their measurements, their implementation can vary. Therefore, we
487 implemented different definitions and methods for most phenotypes, see Suppl. Text “Methods for phenotype
488 extraction” and Suppl. Text “Correlation structure and heritability of extended list of retinal vascular IDPs”.
489 In this study, we focused on 17 representative phenotypes with significant heritability and relevant disease

490 associations. These phenotypes were selected for independence, removing highly redundant phenotypes with
491 similar definitions, but keeping some highly correlated phenotypes when they resulted from significantly
492 different definitions. The mean between left and right eye measurements was taken whenever measurements
493 from both eyes passed quality control, otherwise, the single eye measurement was used. Measurements
494 from only the first measured time point were used whenever measurements from multiple time points were
495 present. Cohen's d , $\frac{\overline{r^{(g)}} - \overline{r^{(p)}}}{\sqrt{\frac{SD^{(g)^2} + SD^{(p)^2}}{2}}}$, was used to quantify the mean difference between genetic and phenotypic
496 correlations.

497 We used two validation procedures: (1) visual inspection of random images in the UKBB to identify and
498 refine potential confounders affecting certain phenotypes, and (2) the use of the DRIVE dataset as a proxy
499 to assess performance in other datasets with similar characteristics, using ground truth on it for the number
500 of bifurcations and temporal angles (Suppl. Text "Validation of IDPs").

501 **Correction for covariates**

502 IDPs were corrected for sex, age, age-squared, sex-by-age, sex-by-age-squared, spherical power, spherical
503 power-squared, cylindrical power, cylindrical power-squared, instance, assessment center, genotype mea-
504 surement batch, and genomic PCs 1-20. Their associations with each phenotype have been visualized in
505 Suppl. Text "Covariate effects". For GWAS, raw phenotypes were transformed with the rank-based inverse
506 normal transformation (rb-INT) before correction.

507 **Disease association**

508 The list of diseases analyzed includes vascular and eye-related diseases, risk factors, mortality, and other
509 conditions previously found to be associated with the retina vascular system. The disease data were collected
510 from the UKBB, and the official datafield identifier corresponding to each disease can be found in the
511 Suppl. Text "Diseases list UKBB", and in Suppl. Data "[Diseases information](#)".

512 Different regression models were employed based on the nature of the disease traits. For risk factors,
513 ordinary least squares (OLS) linear regression was used to estimate standardized effects using the 'statsmod-
514 els.formula.api' library in Python 3.8.13. For binary and categorical disease phenotypes, logistic regression
515 was applied, using the logit function from the 'statsmodels.formula.api' library.

516 Prior to conducting the regression analyses, a pre-processing step was performed to address potential con-
517 founding effects. Covariates were regressed out of retinal IDPs and the obtained residuals were then used as
518 regressors in the linear/logistic regression analyses. For Cox models, the covariates were added again to the
519 models to adjust for potential non-linear effects.

520 The regression models were fitted using the adjusted independent variables, the estimates of regression
521 coefficients (betas), and their corresponding standard deviation (std), or odds ratios were obtained. To
522 determine the significance of regression coefficients, p-values were computed and compared to predefined

523 alpha thresholds (0.05 and 0.001), divided by the total number of tests conducted (i.e., the number of
524 independent variables multiplied by the number of diseases analyzed).

525 In cases where time-to-event data was available and accurate diagnosis was feasible, multivariate Cox pro-
526 portional hazards regression was utilized. This approach allowed us to estimate hazard ratios for diseases
527 with time-to-event outcomes and reliable diagnoses. ‘coxph’ from the R packages ‘survival’ and ‘survminer’
528 were used with default parameters.

529 **Genome-wide analyses**

530 GWAS for UKBB data was performed using BGENIE [73]. SNP-wise heritabilities and genetic correlations
531 between IDPs were derived using LDSR [52]. Gene and pathway scores were computed using *PascalX* [54, 74].
532 Both protein-coding genes and lincRNAs were scored using the novel, approximate “saddle” method, taking
533 into account all SNPs within a 50kb window around each gene. All pathways available in MSigDB v7.2 were
534 scored using *PascalX* ranking mode, fusing and rescoreing any co-occurring genes less than 100kb apart.
535 *PascalX* requires LD structure to accurately compute gene scores, which in our analyses was provided with
536 the UK10K (hg19) reference panel. Gene-level cross-GWAS coherence test between IDP pairs and between
537 IDPs and diseases or risk factors was computed using the *PascalX* cross-scoring *zsum* method, testing for
538 both coherence and anti-coherence of GWAS signals. Variants with a minor allele frequency of at least 0.001
539 were considered. Correction for bias due to sample overlap was done using the intercept from pairwise LDSR
540 genetic correlation. The significance threshold was set at 0.05 divided by the number of tested genes. Top
541 hits GWAS summary statistics can be found in Suppl. Data “[GWAS top hits \(UKBB\) before pruning](#)”.

542 **Genetic association with diseases**

543 For the genetic correlation between IDPs and diseases, the summary statistics of the diseases in LDSR format
544 were obtained from the Neale lab ([nealelab-ldsc-sumstat-files](#)). LDSR was computed for the diseases and the
545 IDPs. We limited ourselves to diseases that were categorized as ‘High confidence’ by the Neale lab (column
546 ‘Neale_ldsr’ in Suppl. Data “[Diseases information](#)”).

547 Regarding the genes shared between IDPs and diseases, we used the GWAS summary statistics for diseases
548 ([nealelab-sumstat-files](#)). However, in this case, we applied some additional filters deleting rsid values that
549 did not start with ‘rs’, p-values that were missing, and low confidence variants (Suppl. Data “[Significant](#)
550 [genes per diseases](#)”).

551 Binary disease states were included in the genetic analysis, however, their results require additional caution,
552 since the GWAS summary statistics from the Neale lab used linear regression for all the disease phenotypes,
553 which is not ideal for non-continuous response variables. It should be noted that the covariates used for the
554 GWAS analysis of our IDPs and those used for the risk factors/diseases are almost, but not exactly, the
555 same (age, sex, age-squared, age-by-sex, age-by-sex-squared, and first 20 PCs for risk factors/diseases).

556 Mendelian Randomisation

557 To perform the bidirectional two-sample MR analyses we used the TwoSamplesMR package in R [57]. We
558 first considered independent SNPs significantly ($p < 5 \times 10^{-8}$) associated with the exposure as genetic
559 instruments, pruning SNPs with $r^2 > 0.001$ to a lead SNP according to LD estimates from the UK10K
560 reference panel [75]. In cases where the number of instruments was below 10, we relaxed the selection
561 threshold for instruments to $p < 10^{-6}$. In general, the number of instruments tended to be lower when using
562 IDPs, rather than disease traits as exposures, which may be due, at least partially, to lower sample sizes. For
563 this reason, when using IDPs as exposures we relaxed the selection threshold for instruments to $p < 10^{-6}$.

564 To assess instrument strength, we computed the F-statistic from the regression of the exposure on the
565 instruments [76] defined as $F = \frac{R^2 \times (N - k - 1)}{(1 - R^2) \times k}$, where R^2 is the explained variance of the exposure by
566 the instruments, N is the sample size of the GWAS for the exposure, and k is the number of instruments.
567 For all the forward and reverse MR pairs, the F-statistics were > 50 suggesting that the selected SNPs were
568 suitable instruments.

569 Causal estimates were based on the inverse variance-weighted method (IVW) [58]. In particular, we used a
570 fixed-effect model when having three or less instruments, and otherwise a random-effects model. To comple-
571 ment and enhance the reliability of the results, we applied additional methods, namely MR-Egger, weighted
572 median, and weighted mode [77, 78] MR. For all exposure-outcome pairs, the estimated causal effects were
573 consistent in the direction across the four methods whenever significant. Differences in significance levels
574 are likely because the power of these additional methods is smaller than that of the IVW method [79]
575 (Suppl. Data “MR risk factors (all methods)”).

576 Notably, MR-Egger intercepts of most of the associations were not significantly different from zero, suggesting
577 that no significant pleiotropy was detected (Suppl. Data “MR risk factors (Egger intercept)”). Lastly, leave-
578 one-out analyses showed that the estimates were not biased by any single SNP (Suppl. Data “MR risk factors
579 (LOO)”). Overall, the sensitivity analyses confirmed the reliability of most of our putative causal effects in
580 both directions.

581 Since the number of UKBB subjects for which we extracted IDPs was much smaller than the number of
582 UKBB subjects used to study disease phenotypes, our analysis can still be considered a two-sample MR
583 setup, and potential bias due to sample overlap is expected to be small and in direction of the null [80, 81].

584 Replication

585 The RS is a prospective population-based cohort study of people living in Ommoord, a district of the city
586 of Rotterdam [82]. The RS consists of four cohorts, all of which were used in this replication. Each cohort
587 was followed for multiple rounds of follow-up examinations every 4 to 5 years. Most of the patient visits
588 in the RS involved the capture of CFIs on both eyes. Due to the multi-decade span of the RS, multiple
589 devices, capture conditions and fields (macula and disc centered) are present in the dataset. In the RS,

590 DNA extraction was performed using whole blood samples following standardized and previously described
591 protocols [82]. Genotyping was performed using both the Infinium II HumanHap550(-Duo) (RS-I & RS-
592 II) and 610-Quad Genotyping BeadChip (RS-I & RS-III; Illumina, San Diego, CA, USA). Imputation of
593 markers was performed using the Haplotype Reference Consortium version 1.1 as the reference panel [83].
594 The CoLaus study, initiated in 2003 in Lausanne, Switzerland, involves over 6 700 volunteers aged 35 to 75.
595 OphtalmoLaus, a segment of CoLaus, delves into ocular health. OphtalmoLaus CFIs were acquired with
596 Topcon 2000 or Topcon triton. The number of initial images was 6 503, corresponding to 2 276 participants.

597 **Phenotyping and cross-correlations**

598 In this study we made use of RS imaging from recent rounds (RS-I-4, RS-II-4, RS-III-1, RS-IV-1) due to the
599 generally higher quality and number of these images, even though in some cases this meant less participants.
600 We quality-controlled the images by automatically filtering out images where the OD was near or out of
601 the bounds of the CFI. Both disc- and macula-centered images were included. After QC, the number of
602 participants with usable images per RS cohort was 2 710 (RS-I), 1 169 (RS-II), 3 350 (RS-III), and 2 658
603 (RS-IV). Most visits in the RS captured multiple CFIs per participant. The average number of usable CFIs
604 per subject varied between 2.96 (RS-I) and 7.75 (RS-IV), including both eyes. A participant's features were
605 computed as the mean over all their images' features.

606 To accommodate the use of disc-centered images and the high variability in imaging conditions present in
607 the RS, we made use of segmentation and feature extraction methods trained and tested on RS data. The
608 17 phenotypes computed for the main study were implemented in a fundus analysis software used in-house
609 following the original implementation.

610 To compute the RS phenotypic cross-correlations in Fig. 7, IDPs were corrected for age, sex, eye geometry,
611 imaging device (if multiple were used within the same cohort, dummy coded), and genomic PCs 1-10. Eye
612 geometry was included as a combination of the spherical and cylindrical powers into one variable as spherical
613 equivalent (spherical power + cylindrical power/2).

614 For OphtalmoLaus, in the case of multiple images for the same participant, we kept the one with the highest
615 QC score. The number of participants after removing the images that failed the segmentation or IDPs
616 computation, and after QC, was N=1 715 participants. If both eyes survived this screening, we averaged out
617 the phenotypes of the two eyes, while if only one eye survived then we considered the phenotypes of that
618 eye. After that, we cross-referenced with the sample file and the final number of subjects was 1 435. We
619 corrected for the following covariates: age, sex, age-by-sex, age-squared, cylindrical and spherical powers,
620 spherical-squared, cylindrical-squared, and genomic PCs 1-10.

621 **GWAS**

622 As imputation and QC of the four RS-cohorts were done separately, we also performed the GWAS anal-
623 yses separately and then meta-analyzed the results. For the initial GWAS analyses, we performed linear

624 regressions using Plink 2.0 [84]. The included covariates were the same as for the phenotypic correlation, i.e.
625 age, sex, eye geometry, imaging device, and genomic PCs 1-10. We performed an inverse variance weighted
626 fixed-effect meta-analysis, using METAL software [85]. P-values for the association results were calculated
627 by using the z-statistic. The meta-analyzed significant hits were pruned using Plink 2.0. Variants were
628 considered independent if they were at least 500 kb apart and had an $R^2 < 0.1$. Top hits GWAS summary
629 statistics in the RS can be found in Suppl. Data “[GWAS top hits \(RS\) before pruning](#)”.

630 **Data and code availability**

631 The genetic and phenotypic UKBB data are available upon application to the UKBB, <https://www.ukbiobank.ac.uk>. Similarly for the replication data, RS and OphthalmoLaus, data can be made available
632 upon request to researchers through a data transfer agreement. GWAS summary statistics will be available
633 on the GWAS Catalog following publication. Code will be made available in our public GitHub repository
634 following publication: <https://github.com/BergmannLab/retina-phenotypes>.

636 **Author contributions**

637 SOV, MJB, and SB designed this study. MJB performed QC and image preprocessing. SOV extracted the
638 number of bifurcations, temporal angles, central retinal equivalents, and diameter variability. MJB extracted
639 OD positions, vascular density, and fractal dimension. MT extracted median diameter and tortuosity. MJB
640 performed postprocessing (covariate correction and normalization). GWAS was performed by MJB and SOV
641 for UKBB data. MJB estimated heritabilities and cross-phenotype correlations. SOV and MJB performed gene
642 and pathway analysis. Gene-level cross-phenotype analysis was done by OT. Linear and logistic regressions
643 were done by SOV and OT, and Cox model analyses by MJB. Cross-phenotype LDSR and gene analysis
644 between retina phenotypes and diseases were done by SOV and OT. FH helped SOV with the validation of
645 the angles and bifurcation phenotypes. II performed MR analysis. JDVQ and VAV performed RS replication
646 under the supervision of WR, BL, and CCWK. IM and AE performed OphthalmoLaus replication under the
647 supervision of MT and RS. SB supervised all analyses. SOV, MJB, OT, II, MT, JDVQ, IM, and SB wrote
648 the manuscript. All other authors contributed to the writing.

649 **Acknowledgements**

650 The authors thank Leah Böttger and Sacha Bors for their valuable comments on the manuscript. The authors
651 thank the entire EyeNED team for their various contributions during the development of the algorithms used
652 in the RS replication. The authors are grateful to the study participants and the staff from the UKBB, RS,
653 and OphthalmoLaus.

654 Funding

655 Supported by the Swiss National Science Foundation grant no. CRSII5_209510 for the “VascX” Sinergia
656 project. Supported by Oogfonds, Stichting voor Ooglijders, Stichting voor Blindenhulp, Henkes stichting,
657 and Landelijke Stichting voor Blinden en Slechtienden (LSBS). Additional support was given by Erasmus
658 Medical Center, Erasmus University, Netherlands Organization for the Health Research and Development
659 (ZonMw), the Research Institute for Diseases in the Elderly (RIDE), the Ministry of Education, Culture
660 and Science, the Ministry for Health, Welfare and Sports, the European Commission (DG XII), and the
661 Municipality of Rotterdam.

662 Conflict of Interest statement: None declared.

663 References

- 664 [1] M Kamran Ikram, Yi Ting Ong, Carol Y Cheung, and Tien Y Wong. Retinal vascular caliber mea-
665 surements: clinical significance, current knowledge and future perspectives. *Ophthalmologica*, 229(3):
666 125–136, 2013.
- 667 [2] Sara B Seidelmann, Brian Claggett, Paco E Bravo, Ankur Gupta, Hoshang Farhad, Barbara E Klein,
668 Ronald Klein, Marcelo Di Carli, and Scott D Solomon. Retinal vessel calibers in predicting long-term
669 cardiovascular outcomes: the atherosclerosis risk in communities study. *Circulation*, 134(18):1328–1338,
670 2016.
- 671 [3] Ryo Kawasaki, Ning Cheung, Jie Jin Wang, Ronald Klein, Barbara EK Klein, Mary Frances Cotch,
672 A Richey Sharrett, Steven Shea, FM Amirul Islam, and Tien Y Wong. Retinal vessel diameters and risk
673 of hypertension: the multiethnic study of atherosclerosis. *Journal of hypertension*, 27(12):2386, 2009.
- 674 [4] M Kamran Ikram, Frank Jan De Jong, Ewoud J Van Dijk, Niels D Prins, Albert Hofman, Monique MB
675 Breteler, and Paulus TVM De Jong. Retinal vessel diameters and cerebral small vessel disease: the
676 rotterdam scan study. *Brain*, 129(1):182–188, 2006.
- 677 [5] Raviv Allon, Michael Aronov, Michael Belkin, Elad Maor, Michael Shechter, and Ido Didi Fabian.
678 Retinal microvascular signs as screening and prognostic factors for cardiac disease: a systematic review
679 of current evidence. *The American Journal of Medicine*, 134(1):36–47, 2021.
- 680 [6] Gerald Liew, Paul Mitchell, Elena Rochtchina, Tien Yin Wong, Wynne Hsu, Mong Li Lee, Alan Wain-
681 wright, and Jie Jin Wang. Fractal analysis of retinal microvasculature and coronary heart disease
682 mortality. *European heart journal*, 32(4):422–429, 2011.
- 683 [7] Maximilian WM Wintergerst, Peyman Falahat, Frank G Holz, Christian Schaefer, Nadjib Schahab,
684 and Robert Finger. Retinal vasculature assessed by octa in peripheral arterial disease. *Investigative*
685 *Ophthalmology & Visual Science*, 61(7):3203–3203, 2020.

- 686 [8] Wayne Smith, Jie Jin Wang, Tien Yin Wong, Elena Rohtchina, Ronald Klein, Stephen R Leeder, and
687 Paul Mitchell. Retinal arteriolar narrowing is associated with 5-year incident severe hypertension: the
688 blue mountains eye study. *Hypertension*, 44(4):442–447, 2004.
- 689 [9] Tien Wong and Paul Mitchell. The eye in hypertension. *The Lancet*, 369(9559):425–435, 2007.
- 690 [10] Carol Yim-lui Cheung, Yingfeng Zheng, Wynne Hsu, Mong Li Lee, Qiangfeng Peter Lau, Paul Mitchell,
691 Jie Jin Wang, Ronald Klein, and Tien Yin Wong. Retinal vascular tortuosity, blood pressure, and
692 cardiovascular risk factors. *Ophthalmology*, 118(5):812–818, 2011.
- 693 [11] Andrea Grosso, Franco Veglio, Massimo Porta, FM Grignolo, and TY Wong. Hypertensive retinopathy
694 revisited: some answers, more questions. *British Journal of Ophthalmology*, 89(12):1646–1654, 2005.
- 695 [12] Tien Yin Wong, Anoop Shankar, Ronald Klein, Barbara EK Klein, and Larry D Hubbard. Prospective
696 cohort study of retinal vessel diameters and risk of hypertension. *bmj*, 329(7457):79, 2004.
- 697 [13] Tien Yin Wong, Ronald Klein, Barbara EK Klein, Stacy M Meuer, and Larry D Hubbard. Retinal
698 vessel diameters and their associations with age and blood pressure. *Investigative ophthalmology &
699 visual science*, 44(11):4644–4650, 2003.
- 700 [14] SB Dimmitt, SM Eames, P Gosling, JNW West, JM Gibson, and WA Littler. Usefulness of ophthal-
701 moscopy in mild to moderate hypertension. *The Lancet*, 333(8647):1103–1106, 1989.
- 702 [15] Harry Leung, Jie Jin Wang, Elena Rohtchina, Tien Y Wong, Ronald Klein, and Paul Mitchell. Impact
703 of current and past blood pressure on retinal arteriolar diameter in an older population. *Journal of
704 hypertension*, 22(8):1543–1549, 2004.
- 705 [16] Jie Jin Wang, Paul Mitchell, Harry Leung, Elena Rohtchina, Tien Yin Wong, and Ronald Klein.
706 Hypertensive retinal vessel wall signs in a general older population: the blue mountains eye study.
707 *Hypertension*, 42(4):534–541, 2003.
- 708 [17] Tien Yin Wong, Ronald Klein, A Richey Sharrett, Bruce B Duncan, David J Couper, Barbara EK
709 Klein, Larry D Hubbard, and F Javier Nieto. Retinal arteriolar diameter and risk for hypertension.
710 *Annals of internal medicine*, 140(4):248–255, 2004.
- 711 [18] Tien Yin Wong, Ronald Klein, A Richey Sharrett, Bruce B Duncan, David J Couper, James M Tielsch,
712 Barbara EK Klein, and Larry D Hubbard. Retinal arteriolar narrowing and risk of coronary heart
713 disease in men and women: the atherosclerosis risk in communities study. *Jama*, 287(9):1153–1159,
714 2002.
- 715 [19] A Richey Sharrett, Larry D Hubbard, Lawton S Cooper, Paul D Sorlie, Rosemary J Brothers, F Javier
716 Nieto, Joan L Pinsky, and Ronald Klein. Retinal arteriolar diameters and elevated blood pressure: the
717 atherosclerosis risk in communities study. *American journal of epidemiology*, 150(3):263–270, 1999.

- 718 [20] SCY Woo, GYH Lip, and PL Lip. Associations of retinal artery occlusion and retinal vein occlusion to
719 mortality, stroke, and myocardial infarction: a systematic review. *Eye*, 30(8):1031–1038, 2016.
- 720 [21] Tyler Hyungtaek Rim, John Seungsoo Han, Jaewon Oh, Dong Wook Kim, Seok-Min Kang, and Eun Jee
721 Chung. Retinal vein occlusion and the risk of acute myocardial infarction development: a 12-year
722 nationwide cohort study. *Scientific reports*, 6(1):1–9, 2016.
- 723 [22] Danielle L Weiler, Carla B Engelke, Anna LO Moore, and Wendy W Harrison. Arteriole tortuosity
724 associated with diabetic retinopathy and cholesterol. *Optometry and Vision Science*, 92(3):384–391,
725 2015.
- 726 [23] Varun Gulshan, Lily Peng, Marc Coram, Martin C Stumpe, Derek Wu, Arunachalam Narayanaswamy,
727 Subhashini Venugopalan, Kasumi Widner, Tom Madams, Jorge Cuadros, et al. Development and vali-
728 dation of a deep learning algorithm for detection of diabetic retinopathy in retinal fundus photographs.
729 *Jama*, 316(22):2402–2410, 2016.
- 730 [24] Muthu Rama Krishnan Mookiah, U Rajendra Acharya, Hamido Fujita, Jen Hong Tan, Chua Kuang
731 Chua, Sulatha V Bhandary, Augustinus Laude, and Louis Tong. Application of different imaging
732 modalities for diagnosis of diabetic macular edema: a review. *Computers in biology and medicine*, 66:
733 295–315, 2015.
- 734 [25] Jie J Wang, Bronwen Taylor, Tien Y Wong, Brian Chua, Elena Rochtchina, Ronald Klein, and Paul
735 Mitchell. Retinal vessel diameters and obesity: a population-based study in older persons. *Obesity*, 14
736 (2):206–214, 2006.
- 737 [26] Dora Elisa Alvarado-Carrillo, Iván Cruz-Aceves, Martha Alicia Hernández-González, and Luis Miguel
738 López-Montero. Robust detection and modeling of the major temporal arcade in retinal fundus images.
739 *Mathematics*, 10(8):1334, 2022.
- 740 [27] Faraz Oloumi, Rangaraj M Rangayyan, and Anna L Ells. A graphical user interface for measurement
741 of temporal arcade angles in fundus images of the retina. In *2012 25th IEEE Canadian Conference on*
742 *Electrical and Computer Engineering (CCECE)*, pages 1–4. IEEE, 2012.
- 743 [28] Álvaro S Hervella, José Rouco, Jorge Novo, Manuel G Penedo, and Marcos Ortega. Deep multi-instance
744 heatmap regression for the detection of retinal vessel crossings and bifurcations in eye fundus images.
745 *Computer Methods and Programs in Biomedicine*, 186:105201, 2020.
- 746 [29] Harry Pratt, Bryan M Williams, Jae Yee Ku, Charles Vas, Emma McCann, Baidaa Al-Bander, Yitian
747 Zhao, Frans Coenen, and Yalin Zheng. Automatic detection and distinction of retinal vessel bifurcations
748 and crossings in colour fundus photography. *Journal of Imaging*, 4(1):4, 2018.
- 749 [30] Xiayu Xu, Joseph M Reinhardt, Qiao Hu, Benjamin Bakall, Paul S Tluczek, Geir Bertelsen, and
750 Michael D Abramoff. Retinal vessel width measurement at branchings using an improved electric field
751 theory-based graph approach. *PloS one*, 7(11):e49668, 2012.

- 752 [31] Alauddin Bhuiyan, Baikunth Nath, and Kotagiri Ramamohanarao. Detection and classification of
753 bifurcation and branch points on retinal vascular network. In *2012 International Conference on Digital*
754 *Image Computing Techniques and Applications (DICTA)*, pages 1–8. IEEE, 2012.
- 755 [32] M Elena Martinez-Perez, Alun D Hughes, Alice V Stanton, Simon A Thom, Neil Chapman, Anil A
756 Bharath, and Kim H Parker. Geometrical and morphological analysis of vascular branches from fundus
757 retinal images. In *Medical Image Computing and Computer-Assisted Intervention–MICCAI 2000: Third*
758 *International Conference, Pittsburgh, PA, USA, October 11-14, 2000. Proceedings 3*, pages 756–765.
759 Springer, 2000.
- 760 [33] Adria Perez-Rovira, T MacGillivray, Emanuele Trucco, KS Chin, K Zutis, C Lupascu, Domenico Tegolo,
761 Andrea Giachetti, Peter J Wilson, A Doney, et al. Vampire: vessel assessment and measurement
762 platform for images of the retina. In *2011 Annual International Conference of the IEEE Engineering*
763 *in Medicine and Biology Society*, pages 3391–3394. IEEE, 2011.
- 764 [34] Behdad Dashtbozorg, Ana Maria Mendonca, Susana Penas, and Aurelio Campilho. Retinacard, a system
765 for the assessment of retinal vascular changes. In *2014 36th Annual International Conference of the*
766 *IEEE Engineering in Medicine and Biology Society*, pages 6328–6331. IEEE, 2014.
- 767 [35] Jonathan Fhima, Jan Van Eijgen, Ingeborg Stalmans, Yevgeniy Men, Moti Freiman, and Joachim A
768 Behar. Pvbmm: A python vasculature biomarker toolbox based on retinal blood vessel segmentation.
769 In *Computer Vision–ECCV 2022 Workshops: Tel Aviv, Israel, October 23–27, 2022, Proceedings, Part*
770 *III*, pages 296–312. Springer, 2023.
- 771 [36] Adrian Galdran, André Anjos, José Dolz, Hadi Chakor, Hervé Lombaert, and Ismail Ben Ayed. State-
772 of-the-art retinal vessel segmentation with minimalistic models. *Scientific Reports*, 12(1):1–13, 2022.
- 773 [37] Artem Sevastopolsky. Optic disc and cup segmentation methods for glaucoma detection with modifi-
774 cation of u-net convolutional neural network. *Pattern Recognition and Image Analysis*, 27(3):618–624,
775 2017.
- 776 [38] Harry Pratt, Bryan M Williams, Jae Yee Ku, Charles Vas, Emma McCann, Baidaa Al-Bander, Yitian
777 Zhao, Frans Coenen, and Yalin Zheng. Automatic detection and distinction of retinal vessel bifurcations
778 and crossings in colour fundus photography. *Journal of Imaging*, 4(1):4, 2017.
- 779 [39] Ziqian Xie, Tao Zhang, Sangbae Kim, Jiaxiong Lu, Wanheng Zhang, Cheng-Hui Lin, Man-Ru Wu,
780 Alexander Davis, Roomasa Channa, Luca Giancarlo, et al. igwas: image-based genome-wide association
781 of self-supervised deep phenotyping of human medical images. *medRxiv*, pages 2022–05, 2022.
- 782 [40] Yukun Zhou, Mark A Chia, Siegfried K Wagner, Murat S Ayhan, Dominic J Williamson, Robbert R
783 Struyven, Timing Liu, Moucheng Xu, Mateo G Lozano, Peter Woodward-Court, et al. A foundation
784 model for generalizable disease detection from retinal images. *Nature*, pages 1–8, 2023.

- 785 [41] Ryan Poplin, Avinash V Varadarajan, Katy Blumer, Yun Liu, Michael V McConnell, Greg S Corrado,
786 Lily Peng, and Dale R Webster. Prediction of cardiovascular risk factors from retinal fundus photographs
787 via deep learning. *Nature Biomedical Engineering*, 2(3):158–164, 2018.
- 788 [42] Tao Li, Wang Bo, Chunyu Hu, Hong Kang, Hanruo Liu, Kai Wang, and Huazhu Fu. Applications of
789 deep learning in fundus images: A review. *Medical Image Analysis*, 69:101971, 2021.
- 790 [43] Xueling Sim, Richard A Jensen, M Kamran Ikram, Mary Frances Cotch, Xiaohui Li, Stuart MacGregor,
791 Jing Xie, Albert Vernon Smith, Eric Boerwinkle, Paul Mitchell, et al. Genetic loci for retinal arteriolar
792 microcirculation. *PloS one*, 8(6):e65804, 2013.
- 793 [44] Richard A Jensen, Xueling Sim, Albert Vernon Smith, Xiaohui Li, Jóhanna Jakobsdóttir, Ching-Yu
794 Cheng, Jennifer A Brody, Mary Frances Cotch, Barbara Mcknight, Ronald Klein, et al. Novel genetic
795 loci associated with retinal microvascular diameter. *Circulation: Cardiovascular Genetics*, 9(1):45–54,
796 2016.
- 797 [45] M Kamran Ikram, Sim Xueling, Richard A Jensen, Mary Frances Cotch, Alex W Hewitt, M Arfan
798 Ikram, Jie Jin Wang, Ronald Klein, Barbara EK Klein, Monique MB Breteler, et al. Four novel loci
799 (19q13, 6q24, 12q24, and 5q14) influence the microcirculation in vivo. *PLoS genetics*, 6(10):e1001184,
800 2010.
- 801 [46] Abirami Veluchamy, Lucia Ballerini, Veronique Vitart, Katharina E Schraut, Mirna Kirin, Harry Camp-
802 bell, Peter K Joshi, Devanjali Relan, Sarah Harris, Ellie Brown, et al. Novel genetic locus influencing
803 retinal venular tortuosity is also associated with risk of coronary artery disease. *Arteriosclerosis, throm-
804 bosis, and vascular biology*, 39(12):2542–2552, 2019.
- 805 [47] Mattia Tomasoni, Michael Johannes Beyeler, Sofia Ortin Vela, Ninon Mounier, Eleonora Porcu, Tanguy
806 Corre, Daniel Krefl, Alexander Luke Button, Hana Abouzeid, Konstantinidis Lazaros, et al. Genome-
807 wide association studies of retinal vessel tortuosity identify numerous novel loci revealing genes and
808 pathways associated with ocular and cardiometabolic diseases. *Ophthalmology Science*, page 100288,
809 2023.
- 810 [48] Xiaofan Jiang, Pirro G Hysi, Anthony P Khawaja, Omar A Mahroo, Zihe Xu, Christopher J Ham-
811 mond, Paul J Foster, Roshan A Welikala, Sarah A Barman, Peter H Whincup, et al. Gwas on retinal
812 vasculometry phenotypes. *Plos Genetics*, 19(2):e1010583, 2023.
- 813 [49] Seyedeh Maryam Zekavat, Vineet K Raghu, Mark Trinder, Yixuan Ye, Satoshi Koyama, Michael C
814 Honigberg, Zhi Yu, Akhil Pampana, Sarah Urbut, Sara Haidermota, Declan P O’Regan, Hongyu Zhao,
815 Patrick T Ellinor, Ayellet V Segrè, Tobias Elze, Janey L Wiggs, James Martone, Ron A Adelman, Nazlee
816 Zebardast, Lucian Del Priore, Jay C Wang, and Pradeep Natarajan. Deep learning of the retina enables
817 phenome- and genome-wide analyses of the microvasculature. *Circulation*, 11 2021. ISSN 1524-4539. doi:
818 10.1161/CIRCULATIONAHA.121.057709. URL <http://www.ncbi.nlm.nih.gov/pubmed/34743558>.

- 819 [50] Peter Bankhead, C Norman Scholfield, J Graham McGeown, and Tim M Curtis. Fast retinal vessel
820 detection and measurement using wavelets and edge location refinement. *PLoS one*, 7(3):e32435, 2012.
- 821 [51] Brendan Bulik-Sullivan, Hilary K Finucane, Verner Anttila, Alexander Gusev, Felix R Day, Po-Ru
822 Loh, ReproGen Consortium, Psychiatric Genomics Consortium, Genetic Consortium for Anorexia Ner-
823 vosa of the Wellcome Trust Case Control Consortium 3, Laramie Duncan, et al. An atlas of genetic
824 correlations across human diseases and traits. *Nature genetics*, 47(11):1236–1241, 2015.
- 825 [52] Brendan K Bulik-Sullivan, Po-Ru Loh, Hilary K Finucane, Stephan Ripke, Jian Yang, Nick Patterson,
826 Mark J Daly, Alkes L Price, and Benjamin M Neale. Ld score regression distinguishes confounding from
827 polygenicity in genome-wide association studies. *Nature genetics*, 47(3):291–295, 2015.
- 828 [53] David Lamparter, Daniel Marbach, Rico Rueedi, Zoltán Kutalik, and Sven Bergmann. Fast and rigor-
829 ous computation of gene and pathway scores from snp-based summary statistics. 2016. doi: 10.1371/
830 journal.pcbi.1004714. URL <http://www2.unil.ch/cbg/index.php?title=PascalTestData>[http://](http://www2.unil.ch/cbg/index.php?title=Pascal)
831 www2.unil.ch/cbg/index.php?title=Pascal.
- 832 [54] Daniel Krefl and Sven Bergmann. Cross-gwas coherence test at the gene and pathway level. *PLoS*
833 *Computational Biology*, 18(9):e1010517, 2022.
- 834 [55] Stephen Burgess, Dylan S Small, and Simon G Thompson. A review of instrumental variable estimators
835 for mendelian randomization. *Statistical methods in medical research*, 26(5):2333–2355, 2017.
- 836 [56] George Davey Smith and Shah Ebrahim. ‘mendelian randomization’: can genetic epidemiology con-
837 tribute to understanding environmental determinants of disease? *International journal of epidemiology*,
838 32(1):1–22, 2003.
- 839 [57] Danielle Rasooly and Chirag J Patel. Conducting a reproducible mendelian randomization analysis
840 using the r analytic statistical environment. *Current protocols in human genetics*, 101(1):e82, 2019.
- 841 [58] Stephen Burgess, Adam Butterworth, and Simon G Thompson. Mendelian randomization analysis with
842 multiple genetic variants using summarized data. *Genetic epidemiology*, 37(7):658–665, 2013.
- 843 [59] Yoav Benjamini and Yosef Hochberg. On the adaptive control of the false discovery rate in multiple
844 testing with independent statistics. *Journal of educational and Behavioral Statistics*, 25(1):60–83, 2000.
- 845 [60] Sebastian M Sodini, Kathryn E Kemper, Naomi R Wray, and Maciej Trzaskowski. Comparison of
846 genotypic and phenotypic correlations: Cheverud’s conjecture in humans. *Genetics*, 209(3):941–948,
847 2018.
- 848 [61] Travis A Meredith. Inherited retinal venous beading. *Archives of Ophthalmology*, 105(7):949–953, 1987.

- 849 [62] Peter L Oliver, Rebecca A Chodroff, Amrit Gosal, Benjamin Edwards, Amanda FP Cheung, Julio
850 Gomez-Rodriguez, Gene Elliot, Lisa J Garrett, Tom Lickiss, Francis Szele, et al. Disruption of visc-
851 2, a brain-expressed conserved long noncoding rna, does not elicit an overt anatomical or behavioral
852 phenotype. *Cerebral Cortex*, 25(10):3572–3585, 2015.
- 853 [63] Manfred Kayser, Fan Liu, A. Cecile J.W. Janssens, Fernando Rivadeneira, Oscar Lao, Kate van Duijn,
854 Mark Vermeulen, Pascal Arp, Mila M. Jhamai, Wilfred F.J. van IJcken, Johan T. den Dunnen, Si-
855 mon Heath, Diana Zelenika, Dominiek D.G. Despriet, Caroline C.W. Klaver, Johannes R. Vingerling,
856 Paulus T.V.M. de Jong, Albert Hofman, Yurii S. Aulchenko, Andre G. Uitterlinden, Ben A. Oostra,
857 and Cornelia M. van Duijn. Three genome-wide association studies and a linkage analysis identify herc2
858 as a human iris color gene. *American Journal of Human Genetics*, 82:411, 2 2008. ISSN 00029297.
859 doi: 10.1016/J.AJHG.2007.10.003. URL [/pmc/articles/PMC2427174/](https://pmc/articles/PMC2427174/)
860 [?report=abstracthttps://www.ncbi.nlm.nih.gov/pmc/articles/PMC2427174/](https://www.ncbi.nlm.nih.gov/pmc/articles/PMC2427174/?report=abstracthttps://www.ncbi.nlm.nih.gov/pmc/articles/PMC2427174/).
- 861 [64] M Kamran Ikram, Frank Jan de Jong, Johannes R Vingerling, Jacqueline CM Witteman, Albert Hof-
862 man, Monique MB Breteler, and Paulus TVM de Jong. Are retinal arteriolar or venular diameters
863 associated with markers for cardiovascular disorders? the rotterdam study. *Investigative ophthalmology*
864 *& visual science*, 45(7):2129–2134, 2004.
- 865 [65] Thomas J MacGillivray, James R Cameron, Qiuli Zhang, Ahmed El-Medany, Carl Mulholland, Ziyang
866 Sheng, Bal Dhillon, Fergus N Doubal, Paul J Foster, Emmanuel Trucco, et al. Suitability of uk biobank
867 retinal images for automatic analysis of morphometric properties of the vasculature. *PLoS One*, 10(5):
868 e0127914, 2015.
- 869 [66] Josef Flammer, Katarzyna Konieczka, Rosa M Bruno, Agostino Virdis, Andreas J Flammer, and Stefano
870 Taddei. The eye and the heart. *European heart journal*, 34(17):1270–1278, 2013.
- 871 [67] WT Longstreth Jr, Emily K Marino Larsen, Ronald Klein, Tien Yin Wong, A Richey Sharrett, David
872 Lefkowitz, and Teri A Manolio. Associations between findings on cranial magnetic resonance imaging and
873 retinal photography in the elderly: the cardiovascular health study. *American journal of epidemiology*,
874 165(1):78–84, 2007.
- 875 [68] Eui Seok Shin, Christine M Sorenson, and Nader Sheibani. Diabetes and retinal vascular dysfunction.
876 *Journal of ophthalmic & vision research*, 9(3):362, 2014.
- 877 [69] MB Sasongko, TY Wong, TT Nguyen, CY Cheung, JE Shaw, and JJ Wang. Retinal vascular tortuosity
878 in persons with diabetes and diabetic retinopathy. *Diabetologia*, 54:2409–2416, 2011.
- 879 [70] Shariq I Sherwani, Haseeb A Khan, Aishah Ekhzaimy, Afshan Masood, and Meena K Sakharkar. Signif-
880 icance of hba1c test in diagnosis and prognosis of diabetic patients. *Biomarker insights*, 11:BMI-S38440,
881 2016.

- 882 [71] Torsten Willenberg, Anette Schumacher, Beatrice Amann-Vesti, Vincenzo Jacomella, Christoph Thal-
883 hammer, Nicolas Diehm, Iris Baumgartner, and Marc Husmann. Impact of obesity on venous hemody-
884 namics of the lower limbs. *Journal of vascular surgery*, 52(3):664–668, 2010.
- 885 [72] Cathie Sudlow, John Gallacher, Naomi Allen, Valerie Beral, Paul Burton, John Danesh, Paul Downey,
886 Paul Elliott, Jane Green, Martin Landray, et al. Uk biobank: an open access resource for identifying
887 the causes of a wide range of complex diseases of middle and old age. *PLoS medicine*, 12(3):e1001779,
888 2015.
- 889 [73] Clare Bycroft, Colin Freeman, Desislava Petkova, Gavin Band, Lloyd T Elliott, Kevin Sharp, Allan
890 Motyer, Damjan Vukcevic, Olivier Delaneau, Jared O’Connell, et al. The uk biobank resource with
891 deep phenotyping and genomic data. *Nature*, 562(7726):203–209, 2018.
- 892 [74] Daniel Krefl, Alessandro Brandulas Cammarata, and Sven Bergmann. PascalX: a Python library for
893 GWAS gene and pathway enrichment tests. *Bioinformatics*, 39(5):btad296, 05 2023. ISSN 1367-4811.
894 doi: 10.1093/bioinformatics/btad296. URL <https://doi.org/10.1093/bioinformatics/btad296>.
- 895 [75] Jie Huang, Bryan Howie, Shane McCarthy, Yasin Memari, Klaudia Walter, Josine L Min, Petr Danecek,
896 Giovanni Malerba, Elisabetta Trabetti, Hou-Feng Zheng, et al. Improved imputation of low-frequency
897 and rare variants using the uk10k haplotype reference panel. *Nature communications*, 6(1):8111, 2015.
- 898 [76] Stephen Burgess, Simon G Thompson, and Crp Chd Genetics Collaboration. Avoiding bias from weak
899 instruments in mendelian randomization studies. *International journal of epidemiology*, 40(3):755–764,
900 2011.
- 901 [77] Jack Bowden, George Davey Smith, and Stephen Burgess. Mendelian randomization with invalid
902 instruments: effect estimation and bias detection through Egger regression. *International Jour-
903 nal of Epidemiology*, 44(2):512–525, 06 2015. ISSN 0300-5771. doi: 10.1093/ije/dyv080. URL
904 <https://doi.org/10.1093/ije/dyv080>.
- 905 [78] Jack Bowden, George Davey Smith, Philip C. Haycock, and Stephen Burgess. Consistent estima-
906 tion in mendelian randomization with some invalid instruments using a weighted median estima-
907 tor. *Genetic Epidemiology*, 40(4):304–314, 2016. doi: <https://doi.org/10.1002/gepi.21965>. URL
908 <https://onlinelibrary.wiley.com/doi/abs/10.1002/gepi.21965>.
- 909 [79] Fernando Hartwig, George Smith, and Jack Bowden. Robust inference in summary data mendelian
910 randomization via the zero modal pleiotropy assumption. *International journal of epidemiology*, 46, 07
911 2017. doi: 10.1093/ije/dyx102.
- 912 [80] Stephen Burgess, Neil M Davies, and Simon G Thompson. Bias due to participant overlap in two-sample
913 mendelian randomization. *Genetic epidemiology*, 40(7):597–608, 2016.

- 914 [81] Bernd Taschler, Stephen M Smith, and Thomas E Nichols. Causal inference on neuroimaging data with
915 mendelian randomisation. *NeuroImage*, 258:119385, 2022.
- 916 [82] M Arfan Ikram, Guy Brusselle, Mohsen Ghanbari, André Goedegebure, M Kamran Ikram, Maryam
917 Kavousi, Brenda C T Kieboom, Caroline C W Klaver, Robert J de Knegt, Annemarie I Luik, Tamar
918 E C Nijsten, Robin P Peeters, Frank J A van Rooij, Bruno H Stricker, André G Uitterlinden, Meike W
919 Vernooij, and Trudy Voortman. Objectives, design and main findings until 2020 from the rotterdam
920 study. *Eur. J. Epidemiol.*, 35(5):483–517, May 2020.
- 921 [83] Shane McCarthy, Sayantan Das, Warren Kretzschmar, Olivier Delaneau, Andrew R Wood, Alexan-
922 der Teumer, Hyun Min Kang, Christian Fuchsberger, Petr Danecek, Kevin Sharp, Yang Luo, Carlo
923 Sidore, Alan Kwong, Nicholas Timpson, Seppo Koskinen, Scott Vrieze, Laura J Scott, He Zhang,
924 Anubha Mahajan, Jan Veldink, Ulrike Peters, Carlos Pato, Cornelia M van Duijn, Christopher E
925 Gillies, Iliaria Gandin, Massimo Mezzavilla, Arthur Gilly, Massimiliano Cocca, Michela Traglia, Andrea
926 Angius, Jeffrey C Barrett, Dorrett Boomsma, Kari Branham, Gerome Breen, Chad M Brummett, Fabio
927 Busonero, Harry Campbell, Andrew Chan, Sai Chen, Emily Chew, Francis S Collins, Laura J Corbin,
928 George Davey Smith, George Dedoussis, Marcus Dorr, Aliko-Eleni Farmaki, Luigi Ferrucci, Lukas Forer,
929 Ross M Fraser, Stacey Gabriel, Shawn Levy, Leif Groop, Tabitha Harrison, Andrew Hattersley, Odd-
930 geir L Holmen, Kristian Hveem, Matthias Kretzler, James C Lee, Matt McGue, Thomas Meitinger,
931 David Melzer, Josine L Min, Karen L Mohlke, John B Vincent, Matthias Nauck, Deborah Nickerson,
932 Aarno Palotie, Michele Pato, Nicola Pirastu, Melvin McInnis, J Brent Richards, Cinzia Sala, Veikko
933 Salomaa, David Schlessinger, Sebastian Schoenherr, P Eline Slagboom, Kerrin Small, Timothy Spector,
934 Dwight Stambolian, Marcus Tuke, Jaakko Tuomilehto, Leonard H Van den Berg, Wouter Van Rhee-
935 nen, Uwe Volker, Cisca Wijmenga, Daniela Toniolo, Eleftheria Zeggini, Paolo Gasparini, Matthew G
936 Sampson, James F Wilson, Timothy Frayling, Paul I W de Bakker, Morris A Swertz, Steven McCarroll,
937 Charles Kooperberg, Annelot Dekker, David Altshuler, Cristen Willer, William Iacono, Samuli Ripatti,
938 Nicole Soranzo, Klaudia Walter, Anand Swaroop, Francesco Cucca, Carl A Anderson, Richard M My-
939 ers, Michael Boehnke, Mark I McCarthy, Richard Durbin, and Haplotype Reference Consortium. A
940 reference panel of 64,976 haplotypes for genotype imputation. *Nat. Genet.*, 48(10):1279–1283, October
941 2016.
- 942 [84] Christopher C Chang, Carson C Chow, Laurent Cam Tellier, Shashaank Vattikuti, Shaun M Purcell,
943 and James J Lee. Second-generation PLINK: rising to the challenge of larger and richer datasets.
944 *Gigascience*, 4(1):7, February 2015.
- 945 [85] Cristen J Willer, Yun Li, and Gonçalo R Abecasis. METAL: fast and efficient meta-analysis of
946 genomewide association scans. *Bioinformatics*, 26(17):2190–2191, September 2010.